

Entanglement Negativity and Defect Extremal Surface

Yilu Shao,^a Ma-Ke Yuan,^a Yang Zhou^{a,b}

^a*Department of Physics and Center for Field Theory and Particle Physics, Fudan University, Shanghai 200433, China*

^b*Peng Huanwu Center for Fundamental Theory, Hefei, Anhui 230026, China*

E-mail: shaoyilu1999@gmail.com, mkyuan19@fudan.edu.cn, yang_zhou@fudan.edu.cn

ABSTRACT: We study entanglement negativity for evaporating black hole based on the holographic model with defect brane. We introduce a defect extremal surface formula for entanglement negativity. Based on partial reduction, we show the equivalence between defect extremal surface formula and island formula for entanglement negativity in $\text{AdS}_3/\text{BCFT}_2$. Extending the study to the model of eternal black hole plus CFT bath, we find that black hole-radiation negativity follows Page curve, black hole-black hole negativity decreases until vanishing, radiation-radiation negativity increases and then saturates at a time later than Page time. In all the time dependent cases, defect extremal formula agrees with island formula.

Contents

1	Introduction	1
2	Review of entanglement negativity in CFT_2	2
2.1	Replica trick for entanglement negativity	2
2.2	Examples of entanglement negativity in CFT_2	3
3	Holographic results and island formula	5
3.1	Holographic computation of entanglement negativity	5
3.2	Island formula for entanglement negativity	6
4	Holographic BCFT model with bulk defect	7
5	Entanglement negativity on bulk defect	10
5.1	Single interval $[0, y]$ on the brane	10
5.2	Single interval $[y_1, y_2]$ on the brane	11
5.3	Adjacent intervals $[y_1, y_2]$ and $[y_2, \infty]$ on the brane	12
5.4	Adjacent intervals $[0, y_2]$ and $[y_2, y_3]$ on the brane	13
6	Defect extremal surface for entanglement negativity	13
6.1	DES: the proposal	14
6.2	Single interval $[0, u]$	14
6.2.1	DES result	14
6.2.2	Island result	15
6.3	Single interval $[u_1, u_2]$	15
6.3.1	DES result	15
6.3.2	Island result	17
6.4	Adjacent intervals $[0, u_2]$ and $[u_2, v_2]$	18
6.4.1	DES result	18
6.4.2	Island result	19
7	Time dependent entanglement negativity in black hole evaporation	19
7.1	Review of the emergence of a 2d eternal black hole	19
7.2	The entanglement negativity between black hole interiors	21
7.2.1	Bulk description	21
7.2.2	Boundary description	23
7.2.3	Time evolution	24
7.3	The entanglement negativity between radiation and black hole	24
7.3.1	Bulk description	24
7.3.2	Boundary description	26
7.3.3	Time evolution	27
7.4	The entanglement negativity between radiation and radiation	27

7.4.1	Bulk description	28
7.4.2	Boundary description	30
7.4.3	Time evolution	33
8	Conclusions and discussions	34
A	OPE structure constant for three point function	35
B	The length formula of L_2	37
C	The length formula of L_5	38

1 Introduction

Significant progress has been made in recent understanding of black hole information paradox [1–3]. In particular the island formula for the radiation gives Page curve [28–30] and therefore maintains unitarity. The development relies on the quantum extremal surface formula for the fine grained entropy, which was inspired from the quantum corrected Ryu-Takayanagi formula in computing holographic entanglement entropy [33–35]. While most of the recent studies have been centered on the von Neumann entropy, we need more detailed information about the quantum state, such as more general entanglement structures, to fully understand the black hole information problem. von Neumann entropy is a unique measure characterizing entanglement between two subsystems A and B for a pure state ψ_{AB} . In this paper we want to study the entanglement between two subsystems in a mixed state. In particular we study entanglement negativity in an evaporating black hole with its Hawking radiation. There are several motivations to do so: First, the entire state of black hole and radiation is not always pure. Second, understanding the rich entanglement structures between subsystems of radiation is probably the key to understand how information escapes from the black hole.

As the analogy of von Neumann entropy for pure states, entanglement negativity is an important measure of entanglement in generally mixed states [4, 5]. The calculation of entanglement negativity in conformal field theories has been developed via the replica trick in [6–9]. The behavior of entanglement negativity was analysed in quantum many body systems [10–20, 54, 55] and in topological field theories [21–25]. The entanglement negativity in large central charge was explored in [50]. Several attempts have been made to understand the holographic dual of entanglement negativity. In $\text{AdS}_3/\text{CFT}_2$, the lesson is that for two adjacent intervals, the holographic dual of entanglement negativity is given by the entanglement wedge cross section (times a constant factor).¹ Based on this, the quantum corrected holographic entanglement negativity and the island formula can be conjectured straightforwardly following the generalizations of holographic entanglement entropy [38, 40].

¹There is also an alternative proposal given by mutual information times a constant factor [61].

In this paper we propose defect extremal surface formula for entanglement negativity in holographic models with defects. Defect extremal surface is defined by extremizing the Ryu-Takayanagi formula corrected by the quantum defect theory [46]. This is interesting when the AdS bulk contains a defect brane or string. The defect extremal surface formula for entanglement negativity is a mixed state generalization of that for entanglement entropy. Based on a decomposition procedure of an AdS bulk with a brane, we demonstrate in this paper the equivalence between defect extremal surface formula and island formula for negativity in AdS₃/BCFT₂. We also compute the evolution of entanglement negativity in evaporating black hole model and find that defect extremal surface formula agrees with island formula.

Note added. While this paper is in completion, we get to know the preprint [71] in arXiv, which has some overlap with this paper.

2 Review of entanglement negativity in CFT₂

Entanglement negativity, or more precisely logarithmic negativity, is a mixed state entanglement measure derived from the positive partial transpose (PPT) criterion for the separability of mixed states. It can be defined as taking the trace norm of the partial transpose of the density matrix.

For a bipartite system, the partial transpose ρ_{AB}^T of a density matrix ρ_{AB} is defined by transposing only one part of the system, namely

$$\langle i_A, j_B | \rho_{AB}^T | k_A, l_B \rangle = \langle i_A, l_B | \rho_{AB} | k_A, j_B \rangle , \quad (2.1)$$

where i_A, j_B, k_A, l_B are bases of the Hilbert space $\mathcal{H}_{A,B}$ of subsystems A and B , and the entanglement negativity is then defined as

$$\mathcal{E}(A : B) = \mathcal{E}(\rho_{AB}) \equiv \log \left| \rho_{AB}^T \right|_1 , \quad (2.2)$$

where $|\mathcal{O}|_1 = \text{Tr} \sqrt{\mathcal{O}\mathcal{O}^\dagger}$ is the trace norm.

2.1 Replica trick for entanglement negativity

It is also possible to calculate entanglement negativity in $(1+1)$ d quantum field theories in analogy with the entanglement entropy by the replica trick.

The trace of the norm of partial transposed density matrix can be written in terms of its eigenvalues

$$\text{Tr} \left| \rho^{T_B} \right| = 1 + 2 \sum_{\lambda_i < 0} |\lambda_i| . \quad (2.3)$$

So the integer power of the partial transposed density

$$\text{Tr} \left(\rho^{T_B} \right)^n = \sum_i \lambda_i^n \quad (2.4)$$

depends on the parity of n . Denote $n_e = 2m$ and $n_o = 2m + 1$ for some integer m . The analytic continuation with n_e and n_o will lead to different results. If we take $n_e \rightarrow 1$, we

get our desired result of $\text{Tr} |\rho^{T_B}|$. If we take $n_o \rightarrow 1$, it only recovers the normalization $\text{Tr} \rho^{T_B} = 1$. This means that the correct way to perform analytic continuation is to consider the even sequence $n_e \rightarrow 1$, i.e.

$$\mathcal{E} = \lim_{n_e \rightarrow 1} \log \text{Tr} \left(\rho^{T_B} \right)^{n_e} . \quad (2.5)$$

To compute (2.5), we can use the replica trick introduced in [6]. Consider the system $AB = A \cup B$ made of two disjoint intervals $[u_1, v_1] \cup [u_2, v_2]$. Sewing n copies of the original system along the branch cut representing subsystems A and B forms a n -sheet Riemann surface. The trace of n -th power of the density matrix $\text{Tr} \rho_{AB}^n$ is the partition function $Z_n / (Z_1)^n$ on this n -sheet Riemann surface, with Z_1 the partition function of one copy of the original system.

The trace of n -th power of the partial transposed density matrix can also be written in terms of branch point twist fields as

$$\text{Tr} \rho_{AB}^n = \langle \mathcal{T}_n(u_1) \bar{\mathcal{T}}_n(v_1) \mathcal{T}_n(u_2) \bar{\mathcal{T}}_n(v_2) \rangle , \quad (2.6)$$

where \mathcal{T}_n and $\bar{\mathcal{T}}_n$ are branch point twist fields with different boundary conditions.

Taking partial transpose of the density matrix ρ_{AB} with respect to the second interval B corresponds to the exchange of row and column indices in B . In the path integral representation, this is equivalent to interchanging the upper and lower edges of the second branch cut in ρ_{AB} . This interchange can be regarded as reversing the order of the column and row indices in the subsystem B .

So $\text{Tr}(\rho_{AB}^{T_B})^n$ is the partition function on the n -sheeted surface obtained by joining cyclically n copies of subsystem A and anti-cyclically of subsystem B . And the n -th power of partial transposed density matrix can be written as

$$\text{Tr} \left(\rho_{AB}^{T_B} \right)^n = \langle \mathcal{T}_n(u_1) \bar{\mathcal{T}}_n(v_1) \bar{\mathcal{T}}_n(u_2) \mathcal{T}_n(v_2) \rangle . \quad (2.7)$$

We note here that throughout this paper, any n appearing in the calculation of entanglement negativity using replica trick shall be automatically regarded as n_e .

2.2 Examples of entanglement negativity in CFT₂

Now we review the results of some examples in conformal field theory. It is known that the conformal weight of twist fields is

$$h_{\mathcal{T}_n} = h_{\bar{\mathcal{T}}_n} \equiv h_n = \frac{c}{24} \left(n - \frac{1}{n} \right) , \quad (2.8)$$

where c is the central charge of the CFT.

Single interval We start with the four-point function in (2.7). Let $v_1 \rightarrow u_2$ and $v_2 \rightarrow u_1$, we have

$$\text{Tr} \left(\rho_{AB}^{T_B} \right)^n = \langle \mathcal{T}_n^2(u_2) \bar{\mathcal{T}}_n^2(v_2) \rangle . \quad (2.9)$$

Setting $n = n_e$, we get

$$\text{Tr} \left(\rho_{AB}^{T_B} \right)^{n_e} = \left(\langle \mathcal{T}_{n_e/2}(u_2) \bar{\mathcal{T}}_{n_e/2}(v_2) \rangle \right)^2 = d_{n_e/2}^2 \left(\frac{u_2 - u_1}{\epsilon} \right)^{-\frac{c}{3} \left(\frac{n_e}{2} - \frac{2}{n_e} \right)} \quad (2.10)$$

with ϵ a UV regulator. d_n is the OPE constant for the two-point function. And finally taking analytic continuation $n_e \rightarrow 1$ leads to

$$\left| \rho_{AB}^{T_B} \right|_1 = \lim_{n_e \rightarrow 1} \text{Tr} \left(\rho_{AB}^{T_B} \right)^{n_e} = d_{1/2}^2 \left(\frac{\ell}{\epsilon} \right)^{c/2} \Rightarrow \mathcal{E} = \frac{c}{2} \log \left(\frac{\ell}{\epsilon} \right) + 2 \log d_{1/2} , \quad (2.11)$$

in which $\ell = u_2 - u_1$ denotes the length of the interval. From [6] we know that for pure state, entanglement negativity equals to Rényi entanglement entropy $S^{(n)}$ of order $1/2$. The latter is given by

$$S^{(n)} = \frac{c}{6} \left(1 + \frac{1}{n} \right) \log \left(\frac{\ell}{\epsilon} \right) . \quad (2.12)$$

With $n \rightarrow 1/2$,

$$S^{(1/2)} = \frac{c}{2} \log \left(\frac{\ell}{\epsilon} \right) . \quad (2.13)$$

Seen from holography [51], the minimal entanglement wedge cross section in this case is the RT surface. We can check that

$$\mathcal{E} = \frac{3}{2} E_W . \quad (2.14)$$

Two adjacent intervals Let $v_1 \rightarrow u_2$ in (2.7), we have

$$\text{Tr} \left(\rho_{AB}^{T_B} \right)^n = \langle \mathcal{T}_n(u_1) \bar{\mathcal{T}}_n^2(u_2) \mathcal{T}_n(v_2) \rangle . \quad (2.15)$$

To keep it simple, set $u_1 = -\ell_1$, $u_2 = 0$ and $v_2 = \ell_2$ and all length are measured in the unit of ϵ . The conformal dimension of the double twist operator \mathcal{T}_n^2 and $\bar{\mathcal{T}}_n^2$ is $h'_n = \frac{c}{12} \left(\frac{n}{2} - \frac{2}{n} \right)$. Taking $n = n_e$ and we get

$$\langle \mathcal{T}_{n_e}(-\ell_1) \bar{\mathcal{T}}_{n_e}^2(0) \mathcal{T}_{n_e}(\ell_2) \rangle = d_{n_e}^2 \frac{C_{\mathcal{T}_{n_e} \bar{\mathcal{T}}_{n_e}^2 \mathcal{T}_{n_e}}}{\ell_1^{2h'_{n_e}} \ell_2^{2h'_{n_e}} (\ell_1 + \ell_2)^{4h'_{n_e} - 2h'_{n_e}}} , \quad (2.16)$$

The OPE structure constant $C_{\mathcal{T}_n \bar{\mathcal{T}}_n^2 \mathcal{T}_n}$ is universal. We can actually fix this constant to be

$$\lim_{n \rightarrow 1} C_{\mathcal{T}_n \bar{\mathcal{T}}_n^2 \mathcal{T}_n} = 2^{c/4} \quad (2.17)$$

by taking the pure state limit of the three-point function (2.16) and compare it with the two-point function (2.11), see appendix A. Taking $n_e \rightarrow 1$ limit and choose the normalization $d_1 = 1$, we have

$$\left| \rho_{AB}^{T_B} \right|_1 \propto \left(\frac{\ell_1 \ell_2}{\ell_1 + \ell_2} \right)^{c/4} \cdot 2^{c/4} \Rightarrow \mathcal{E} = \frac{c}{4} \log \frac{\ell_1 \ell_2}{(\ell_1 + \ell_2) \epsilon} + \frac{c}{4} \log 2 . \quad (2.18)$$

Recall the entanglement wedge cross section [41]

$$E_W = \begin{cases} \frac{c}{6} \log \frac{1+\sqrt{x}}{1-\sqrt{x}} , & \frac{1}{2} \leq x \leq 1 \\ 0 , & 0 \leq x \leq \frac{1}{2} \end{cases} \quad (2.19)$$

with x the cross-ratio

$$x = \frac{\ell_1 \ell_2}{(\ell_1 + d)(\ell_2 + d)} , \quad (2.20)$$

in which d is the distance between two intervals. To recover adjacent interval limit, one can take $d = 2\epsilon \rightarrow 0$,

$$E_W \rightarrow \frac{c}{6} \log \left(\frac{2}{\epsilon} \frac{\ell_1 \ell_2}{(\ell_1 + \ell_2)} \right) . \quad (2.21)$$

This again supports the relation

$$\mathcal{E} = \frac{3}{2} E_W . \quad (2.22)$$

For the more general two disjoint intervals the entanglement negativity depends on four-point function of a CFT, and it is challenging to compute and in most cases non-universal. Numerical methods are often required. In [6], the asymptotic behavior of entanglement negativity of two disjoint intervals is studied. In the limit of $x \rightarrow 1$, the entanglement negativity is $\mathcal{E} \simeq -\frac{c}{4} \log(1-x)$. Following the monodromy method of Hartman [39], the authors of [50] recovers this result in the large central charge limit.

3 Holographic results and island formula

3.1 Holographic computation of entanglement negativity

Kudler-Flam and Ryu proposed that the holographic dual of CFT logarithmic negativity $\mathcal{E}(A : B)$ is proportional to the entanglement wedge cross section in the classical gravity limit of AdS/CFT [51, 52]. They provided a derivation of the holographic dual of logarithmic negativity based on the observation that $n = 1/2$ Rényi reflected entropy and entanglement negativity may coincide in the large central charge limit of CFT₂

$$\mathcal{E} = \frac{1}{2} S_R^{(1/2)} , \quad (3.1)$$

in which $S_R^{(n)}$ is the Rényi reflected entropy of index n . It is therefore conjectured that the negativity has a holographic dual which is proportional to the area of the wedge cross section Γ in the dual AdS space

$$\mathcal{E} = \frac{3}{2} E_W = \frac{3}{2} \frac{\text{Area}[\Gamma]}{4G_N} . \quad (3.2)$$

Several checks have been done to support the conjectured formula (3.2):

- In [51], the results from holographic calculations agree with the CFT results derived by monodromy method in [50] near $x \sim 1$.
- In [52], the four-point function of twist operators are calculated using the Zamolodchikov recursion relation numerically and they find that the negativity matches the entanglement wedge cross section to a high precision.

However, as pointed out by Dong, Qi and Walter in [53], the above derivation assumes the dominance of replica symmetric saddle. In general the replica non-symmetric saddle could dominate, which may take the holographic dual of logarithmic negativity for two disjoint intervals away from the wedge cross section. In this paper we will restrict ourselves to adjacent two intervals.

Kudler-Flam and Ryu also conjectured the quantum corrected logarithmic negativity formula

$$\mathcal{E}(A : B) = \frac{3}{2} \frac{\langle \mathcal{A}[\partial a \cap \partial b] \rangle_{\tilde{\rho}_{ab}}}{4G_N} + \mathcal{E}^{\text{bulk}}(a : b) + \mathcal{O}(G_N), \quad (3.3)$$

where the entanglement wedge of AB is divided into two regions a, b by the cross section $\partial a \cap \partial b$, and \mathcal{A} is the area operator.² $\mathcal{E}^{\text{bulk}}(a : b)$ is the logarithmic negativity for the density matrix $\tilde{\rho}_{ab}$ of the bulk field theory, shown in fig.1.

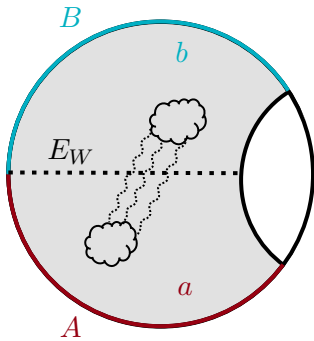


Figure 1: Schematic picture of quantum corrections to entanglement negativity (3.2). The quantum corrections come from bulk matters.

The quantum corrected logarithmic negativity formula (3.3) is similar to the Faulkner, Lewkowycz and Maldacena (FLM) formula of entanglement entropy [37]. Notice that FLM formula only computes the first two orders as an approximation. Engelhardt and Wall proposed that holographic entanglement entropy can be calculated exactly [38] in bulk Plank constant using the so called “quantum extremal surface (QES)” which extremizes the generalized entropy (which coincides with FLM if evaluated on the classical minimal surface).³ In the same spirit, it is tempting to conjecture a quantum extremal cross section which can provide exact result for logarithmic negativity. This leads us to the QES formula for logarithmic negativity

$$\mathcal{E}(A : B) = \text{ext}_{Q'} \left\{ \frac{3}{2} \frac{\text{Area}(Q' = \partial a \cap \partial b)}{4G_N} + \mathcal{E}^{\text{bulk}}(a : b) \right\}, \quad (3.4)$$

where the quantum extremal cross section is denoted by Q' . We emphasize that A and B are adjacent intervals.

3.2 Island formula for entanglement negativity

Recently it has been proposed that QES formula can compute the fine-grained entropy not only for subregions of holographic CFT states but also for more general gravitational systems including black holes and quantum systems coupled with gravity. See [32] for a recent discussion on the fine-grained gravitational entropy. Specifically, the fine-grained

²Here we focus on the static case and employ quantum extremal surface (instead of RT surface of AB) to define the entanglement wedge of AB .

³See [43] for further discussions.

entropy of AdS black hole surround by matter is given by the gravitational generalization of QES,

$$S_B = \text{ext}_Q \left\{ \frac{\text{Area}(Q)}{4G_N} + S(\tilde{\rho}_B) \right\}, \quad (3.5)$$

where Q is the quantum extremal surface, and $\tilde{\rho}_B$ is the matter density matrix. For a quantum system coupled to gravity, such as the CFT bath in the recent 2d JT gravity+CFT model of black hole evaporation, the von Neumann entropy of bath CFT is given by

$$S(\rho_R) = \text{ext}_I \left\{ \frac{\text{Area}(\partial I = Q)}{4G_N} + S(\tilde{\rho}_{R \cup I}) \right\}. \quad (3.6)$$

Importantly, an island contribution has to be included, which can be justified by the gravitational path integral calculation of the von Neumann entropy [30, 36]. If there is more than one extremum, then Q is the surface with minimal entropy. The formula (3.5) can be considered as the black hole version of the original QES and (3.6) can be considered as the radiation version of QES.

Given that there is a QES formula for logarithmic negativity, it is tempting to find similar generalizations to gravitational system. In later sections we will discuss explicitly the two-dimensional eternal black hole + CFT model of black hole evaporation. The eternal black hole + CFT model provides a natural framework to establish the generalizations of QES formula for logarithmic negativity. In fact, a black hole version of that can be easily written down

$$\mathcal{E}(B_L : B_R) = \min \text{ext}_{Q'} \left\{ \frac{3}{2} \frac{\text{Area}(Q' = \partial b_L \cap \partial b_R)}{4G_N} + \mathcal{E}(\tilde{\rho}_{b_L} : \tilde{\rho}_{b_R}) \right\}, \quad (3.7)$$

where b_L and b_R are the entanglement wedges for left black hole and right black hole respectively. Accordingly the island formula of logarithmic negativity for radiation is

$$\mathcal{E}(A : B) = \min \text{ext}_{Q'} \left\{ \frac{3}{2} \frac{\text{Area}(Q' = \partial \text{Is}(A) \cap \partial \text{Is}(B))}{4G_N} + \mathcal{E}(A \cup \text{Is}(A) : B \cup \text{Is}(B)) \right\}. \quad (3.8)$$

We emphasize again that A and B are adjacent intervals. We leave more detail discussions about island formula of logarithmic negativity to sec.6 and sec.7. We also note that in [70], the island formula is obtained by considering the Rényi reflected entropy in large c limit through (3.1).⁴

4 Holographic BCFT model with bulk defect

In [42], Takayanagi proposed a holographic dual for $d = 2$ BCFT by considering a classical AdS₃ geometry with a boundary codimension-one brane Q . The Neumann boundary condition is imposed on the brane. The bulk action is given by

$$I = \frac{1}{16\pi G_N} \int_N \sqrt{-g}(R - 2\Lambda) + \frac{1}{8\pi G_N} \int_Q \sqrt{-h}(K - T), \quad (4.1)$$

⁴See also related works [58–69, 71–73].

where N denotes the bulk and Q the brane. The Neumann boundary condition on the brane with a constant tension T reads

$$K_{ab} = (K - T)h_{ab} , \quad (4.2)$$

where h_{ab} is the induced metric and K_{ab} is the extrinsic curvature of the Q brane. The metric of AdS₃ geometry can be written as

$$\begin{aligned} ds^2 &= d\rho^2 + \cosh^2 \frac{\rho}{l} \cdot ds_{\text{AdS}_2}^2 \\ &= d\rho^2 + l^2 \cosh^2 \frac{\rho}{l} \cdot \frac{-dt^2 + dy^2}{y^2} , \end{aligned} \quad (4.3)$$

where l is the AdS radius. The Poincare metric of AdS₃ can be recovered by replacing the coordinates (ρ, y) with (x, z) via

$$z = -y / \cosh \frac{\rho}{l} , \quad x = y \tanh \frac{\rho}{l} . \quad (4.4)$$

If the Q brane is at $\rho = \rho_0$ with ρ_0 a positive constant, it can be calculated that

$$K_{ab} = \frac{\tanh\left(\frac{\rho_0}{l}\right)}{l} h_{ab} . \quad (4.5)$$

Thus, by combining (4.2) with (4.5), one can determine the relation between the tension T and ρ_0 , i.e.

$$T = \frac{\tanh\left(\frac{\rho_0}{l}\right)}{l} . \quad (4.6)$$

It is also convenient to choose the polar coordinate θ with $\frac{1}{\cos\theta} = \cosh(\rho/l)$. Then, the brane is located at

$$\theta_0 = \arccos \left[\cosh\left(\frac{\rho_0}{l}\right) \right]^{-1} > 0 . \quad (4.7)$$

The boundary entropy can be evaluated from the disk partition function. The difference of the partition function between $\rho = 0$ and $\rho = \rho_0$ is given by $I_E(\rho_0) - I_E(0) = -\frac{\rho_0}{4G_N}$. Then we obtain the boundary entropy

$$S_{\text{bdy}} = \frac{\rho_0}{4G_N} . \quad (4.8)$$

Now we introduce the Holographic BCFT model with bulk defect. This model is inspired by the work of Almheiri, Mahajan, Maldacena and Zhao [29] but the way we treat the theory on the brane is different. We do not replace the matter in the gravity region by its holographic dual. Instead, we treat it as the defect theory on the brane embedded in the bulk. The 2d gravity on the brane comes completely from the Randall-Sundrum reduction of the bulk.

Similar to [29], our model has three alternative descriptions:

- 2d-Gravity: A 2d CFT + gravity theory living on $x < 0$ coupled to a 2d CFT living on $x > 0$. Note that the gravity is obtained by Randall-Sundrum reduction and the CFT is regarded as bulk defect.

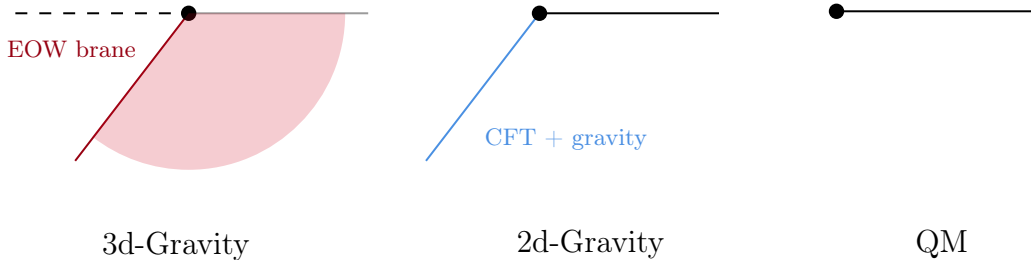


Figure 2: Three different descriptions of the holographic BCFT model. The first is a 3d gravity theory with the AdS_3 bulk. It also contains a bulk defect (EOW brane). The second is a 2d CFT + gravity coupled to a bath CFT_2 on the boundary. The gravitational theory comes from the Randall-Sundrum reduction of some part of the bulk. The third is the fully quantum mechanical description, where we replace the 2d CFT + gravity theory by its quantum mechanical dual.

- 3d-Gravity: A 3d gravity theory in AdS_3 with a bulk defect (End-Of-the-World brane) on part of the space ($x < 0$), and with a rigid AdS boundary on the rest ($x > 0$).
- QM: A two-dimensional CFT on the half-line $x > 0$ with some non-conformal boundary degrees of freedom at $x = 0$. This description should be viewed as the fundamental one.

Now we describe how to change from the 3d-gravity description to the 2d-gravity description via partial reduction and AdS/CFT correspondence. In the BCFT model, the EOW brane should be treated as a part of the bulk. Here we impose Neumann boundary condition so that the matter on the brane contact with bulk gravity through boundary condition. As discussed in [46], an exact deformation of bulk matter to the BCFT is hard to describe, but an effective description is valid.

The way is to use the brane world reduction, or the Randall-Sundrum reduction [45]. In this procedure, the effective Newton constant on the brane is obtained by doing a Randall-Sundrum reduction along the extra dimension, and the $2d$ gravity theory on Q comes from the reduction of the $3d$ bulk. Together with the brane matter on Q , we get the full $2d$ brane theory to be a gravity theory with CFT on the brane. The boundary condition between the brane theory and the half-space CFT should be transparent. Details of this reduction can be found in [46].

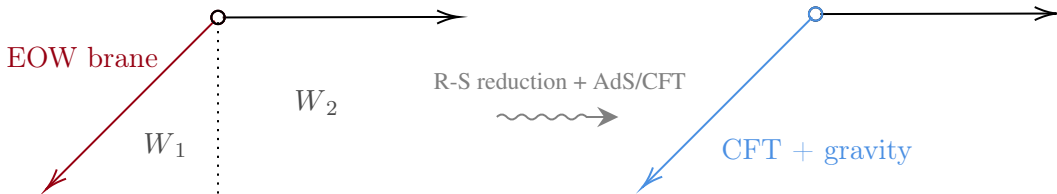


Figure 3: The effective description with R-S reduction in which the bulk W_2 is dual to a flat BCFT, and W_1 is reduced to the EOW brane.

The effective Newton constant on the EOW brane is

$$\frac{1}{4G_N^{(2)}} = \frac{\rho_0}{4G_N} = \frac{c}{6} \operatorname{arctanh}(\sin \theta_0) . \quad (4.9)$$

This is interpreted as boundary entropy (4.8) in the original AdS/BCFT proposal [42].

5 Entanglement negativity on bulk defect

Now we return to the 3d gravity description and calculate the entanglement negativity on bulk defect. If the tension of the EOW brane Q is zero, the EOW brane will be orthogonal to the asymptotic boundary. By adding matter or turn on the tension in the viewpoint of [42], the EOW brane can move to a position with constant angle θ_0 . According to [30], the CFT on AdS_2 can be mapped to a BCFT in flat space via a Weyl transformation. The Weyl factor can be read from the induced metric on the brane $ds_{\text{brane}}^2 = \Omega^{-2}(y) ds_{\text{flat}}^2$, i.e.

$$\Omega(y) = \left| \frac{y \cos \theta_0}{l} \right| . \quad (5.1)$$

5.1 Single interval $[0, y]$ on the brane

From [8], the calculation of a single interval $[0, y]$ including the boundary point means considering the one-point function of the double twist operator \mathcal{T}_n^2 inserted at y . The conformal invariance fixes the form of one-point function on a flat BCFT and by the analysis of twist operators in [8, 44],

$$\langle \mathcal{T}_n^2(y) \rangle_{\text{flat}} = \langle \mathcal{T}_{n/2}(y) \rangle_{\text{flat}}^2 = \frac{g_n}{|2y/\epsilon_y|^{2h'_n}} , \quad (5.2)$$

with ϵ_y the UV cut-off on the brane.

From Weyl transformation (5.1), the one-point function on the brane Q is

$$\langle \mathcal{T}_n^2(y) \rangle_Q = \left| \frac{y \cos \theta_0}{l} \right|^{2h'_n} \langle \mathcal{T}_n^2(y) \rangle_{\text{flat}} = g_n \left| \frac{\epsilon_y \cos \theta_0}{2l} \right|^{2h'_n} . \quad (5.3)$$

Finally, the entanglement negativity on the brane is obtained by taking $n \rightarrow 1$ of the brane one-point function

$$\begin{aligned} \mathcal{E}_{\text{defect}} &= \lim_{n \rightarrow 1} \log \langle \mathcal{T}_n^2(y) \rangle_Q \\ &= \frac{c}{4} \log \frac{2l}{\epsilon_y \cos \theta_0} + \log g . \end{aligned} \quad (5.4)$$

For the boundary without physical degrees of freedom, we set $\log g = 0$. Notice that in this case the entanglement negativity on the brane is a constant and does not depend on the length of the interval.

5.2 Single interval $[y_1, y_2]$ on the brane

Now we derive the the entanglement negativity on the brane for a single interval $[y_1, y_2]$. Following [8] we insert two double twist operators \mathcal{T}_n^2 and $\bar{\mathcal{T}}_n^2$ at $y = y_1$ and $y = y_2$ respectively. Applying Weyl transformation, the two-point function is given by

$$\langle \mathcal{T}_n^2(y_1) \bar{\mathcal{T}}_n^2(y_2) \rangle_Q = \left| \frac{y_1 \cos \theta_0}{l} \right|^{2h'_n} \left| \frac{y_2 \cos \theta_0}{l} \right|^{2h'_n} \langle \mathcal{T}_n^2(y_1) \bar{\mathcal{T}}_n^2(y_2) \rangle_{\text{flat}} . \quad (5.5)$$

Using the doubling trick, this two-point function in the UHP can be seen as a four-point function in the full plane. Employing the same trick developed in [44] for BCFT entanglement entropy, one can find analytical results in the large central charge limit.

Inspired by the holographic calculation [39, 40, 44], we expect that the two-point function has two possible dominate channels: the *operator product expansion channel* (OPE) and the *boundary operator expansion channel* (BOE). This corresponds to different way of doing operator product expansion, see [44]. The dominant channel can be determined by the cross-ratio

$$\eta(y_1, y_2) = \frac{4y_1 y_2}{(y_1 - y_2)^2} . \quad (5.6)$$

From the holographic side, this two channel endures a phase transition due to the change of RT surface from the connected phase to the disconnected phase.

OPE channel If $\eta \rightarrow \infty$, the OPE channel dominates. The corresponding two point function is

$$\langle \mathcal{T}_n^2(y_1) \bar{\mathcal{T}}_n^2(y_2) \rangle_{\text{flat}} = \frac{\epsilon_y^{4h'_n}}{(y_1 - y_2)^{4h'_n}} , \quad (5.7)$$

The entanglement negativity is derived from (5.5):

$$\mathcal{E}_{\text{defect}} = \frac{c}{4} \log \frac{l^2 (y_1 - y_2)^2}{y_1 y_2 \epsilon_y^2 \cos^2 \theta_0} . \quad (5.8)$$

BOE channel If $\eta \rightarrow 0$, the BOE channel dominates. The corresponding two point function is

$$\langle \mathcal{T}_n^2(y_1) \bar{\mathcal{T}}_n^2(y_2) \rangle_{\text{flat}} = \frac{g_b^{4(1-n/2)} \epsilon_y^{4h'_n}}{(4y_1 y_2)^{2h'_n}} . \quad (5.9)$$

The entanglement negativity is derived from (5.5):

$$\mathcal{E}_{\text{defect}} = \frac{c}{2} \log \frac{2l}{\epsilon_y \cos \theta_0} . \quad (5.10)$$

By the same analysis in [46], in the large central charge limit, OPE channel dominates when $\eta \rightarrow \infty$, otherwise the BOE channel dominates. Equating these two results, we have the phase transition point at $\eta = 1$.

5.3 Adjacent intervals $[y_1, y_2]$ and $[y_2, \infty]$ on the brane

For adjacent intervals on brane, we need to consider a different boundary two-point function. We insert \mathcal{T}_n and $\bar{\mathcal{T}}_n^2$ at $y = y_1$ and $y = y_2$ respectively. The two-point function would be

$$\langle \mathcal{T}_n(y_1) \bar{\mathcal{T}}_n^2(y_2) \rangle_Q = \left| \frac{y_1 \cos \theta_0}{l} \right|^{2h_n} \left| \frac{y_2 \cos \theta_0}{l} \right|^{2h'_n} \langle \mathcal{T}_n(y_1) \bar{\mathcal{T}}_n^2(y_2) \rangle_{\text{flat}} . \quad (5.11)$$

BOE channel By the same analysis as above we break the two-point function into product of two one-point function, so the method in [44] still works. The result reads

$$\langle \mathcal{T}_n(y_1) \bar{\mathcal{T}}_n^2(y_2) \rangle_{\text{flat}} = \frac{g_b^{(3-2n)} \epsilon_y^{2h_n+2h'_n}}{(2y_1)^{2h_n} (2y_2)^{2h'_n}} . \quad (5.12)$$

And the entanglement negativity is

$$\mathcal{E}_{\text{defect}} = \frac{c}{4} \log \frac{2l}{\epsilon_y \cos \theta_0} . \quad (5.13)$$

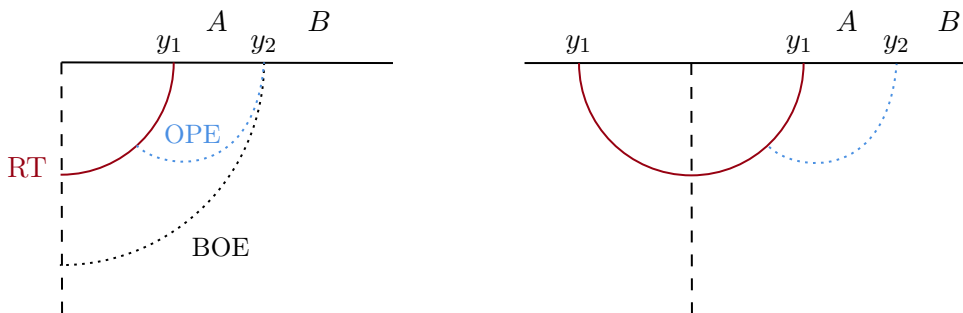


Figure 4: Left: The holographic illustration of possible channels. The boundary point of the brane BCFT is dual to an End-of-the-World brane represented by the dashed vertical line. The RT surface for $A \cup B$ is represented by the red arc. From the field theory side, the BOE channel corresponds to a product of two one-point BCFT correlators. Right: The OPE channel of the two-point BCFT correlator is equivalent to a three-point function on a whole CFT, via the doubling trick.

OPE channel For the simple case in which there is no degree of freedom on the boundary point, we can evaluate the analytic results by making use of the doubling trick. The doubling trick maps a BCFT to a chiral CFT on the flat plane. Then it is equivalent to compute a three point function,

$$\langle \mathcal{T}_n(y_1) \bar{\mathcal{T}}_n^2(y_2) \rangle_{\text{BCFT}} = \langle \mathcal{T}_n(-y_1) \mathcal{T}_n(y_1) \bar{\mathcal{T}}_n^2(y_2) \rangle . \quad (5.14)$$

Simple CFT calculation leads to

$$\langle \mathcal{T}_n(-y_1) \mathcal{T}_n(y_1) \bar{\mathcal{T}}_n^2(y_2) \rangle = \frac{2^{c/4} (2y_1)^{-4h+2h'} \epsilon_y^{2h'}}{(y_2 - y_1)^{2h'} (y_2 + y_1)^{2h'}} . \quad (5.15)$$

The effective entanglement negativity is then obtained,

$$\mathcal{E}_{\text{defect}} = \frac{c}{4} \log \frac{2l}{\xi \epsilon_y \cos \theta_0} \quad (5.16)$$

with

$$\xi = \frac{2y_2 y_1}{y_2^2 - y_1^2} . \quad (5.17)$$

Note that the ξ defined here is slightly different from the ordinary cross-ratio. The valid regime of the two channels can be determined by a critical value ξ_c at which the dominant channel switches to the other. Thus, it is easy to show that OPE channel dominates when $\xi > 1$, otherwise the BOE channel dominates, assuming large central charge limit.

5.4 Adjacent intervals $[0, y_2]$ and $[y_2, y_3]$ on the brane

Following the previous twist operator calculation, we insert $\bar{\mathcal{T}}_n^2$ and \mathcal{T}_n at $y = y_2$ and $y = y_3$ respectively. The two-point function would be:

$$\langle \bar{\mathcal{T}}_n^2(y_2) \mathcal{T}_n(y_3) \rangle_Q = \left| \frac{y_2 \cos \theta_0}{l} \right|^{2h'_n} \left| \frac{y_3 \cos \theta_0}{l} \right|^{2h_n} \langle \bar{\mathcal{T}}_n^2(y_2) \mathcal{T}_n(y_3) \rangle_{\text{flat}} . \quad (5.18)$$

BOE channel The two-point function is given by

$$\langle \bar{\mathcal{T}}_n^2(y_2) \mathcal{T}_n(y_3) \rangle_{\text{flat}} = \frac{g_b^{(3-2n)} \epsilon_y^{2h'_n + 2h_n}}{(2y_2)^{2h'_n} (2y_3)^{2h_n}} \quad (5.19)$$

as above, thus the entanglement negativity for BOE channel is

$$\mathcal{E}_{\text{defect}} = \frac{c}{4} \log \frac{2l}{\epsilon_y \cos \theta_0} . \quad (5.20)$$

OPE channel In this channel the entanglement negativity is

$$\mathcal{E}_{\text{defect}} = \frac{c}{4} \log \frac{2l}{\xi \epsilon_y \cos \theta_0} \quad (5.21)$$

with

$$\xi = \frac{2y_3 y_2}{y_3^2 - y_2^2} , \quad (5.22)$$

and the phase transition point is also at $\xi = 1$.

6 Defect extremal surface for entanglement negativity

In this section, we will propose the defect extremal surface formula for entanglement negativity and compare the DES results and island formula in single interval and adjacent intervals.

6.1 DES: the proposal

In the 3d gravity description, we consider a quantum theory living on the defect which is regarded as a part of the full bulk theory since it is coupled to the bulk. When the classical RT surface intersects with the defect or terminates on the defect, the defect theory should contribute to the entanglement negativity. Following the idea of [46] we propose the *defect extremal surface* formula for entanglement negativity including defect contribution

$$\mathcal{E}_{\text{DES}} = \min_{\Gamma, X} \left\{ \text{ext}_{\Gamma, X} \left[\frac{3}{2} \frac{\text{Area}(\Gamma)}{4G_N} + \mathcal{E}_{\text{defect}}[D] \right] \right\}, \quad X = \Gamma \cap D, \quad (6.1)$$

where Γ is a co-dimension two surface in AdS_3 and X is the lower dimensional entangling surface given by the intersection of Γ and D . $\mathcal{E}_{\text{defect}}$ is the entanglement negativity on bulk defect, which is derived in the previous section.

6.2 Single interval $[0, u]$

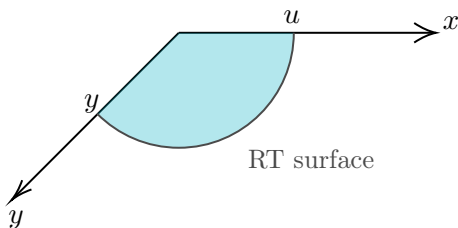


Figure 5: The case of a single interval $[0, u]$. The blue area denotes the entanglement wedge.

6.2.1 DES result

In this case we consider a single interval which contains the boundary point. The RT surface can only end on the brane, as shown in fig.5. Assuming the intersection point of the RT surface and the brane is y , the bulk defect of $[0, y]$ can be derived from the same geometric analysis in [46]. We denote

$$u' = \frac{y^2 + u^2 + 2yu \sin \theta}{2(u + y \sin \theta)}, \quad (6.2)$$

$$\theta' = \arcsin \frac{u^2 + 2yu \sin \theta - y^2 \cos 2\theta}{u^2 + 2yu \sin \theta + y^2}. \quad (6.3)$$

The generalized entanglement negativity is given by considering both contributions

$$\mathcal{E}_{\text{gen}}(y) = \mathcal{E}_{\text{area}} + \mathcal{E}_{\text{defect}} = \frac{c}{4} \log \frac{2u'}{\epsilon_u} + \frac{c}{4} \text{arctanh}(\sin \theta'_0) + \frac{c'}{4} \log \frac{2l}{\epsilon_y \cos \theta_0}. \quad (6.4)$$

where $\theta'_0 = \theta'|_{\theta=\theta_0}$ and we used the single interval bulk defect result (5.4).

In order to extremize $\mathcal{E}_{\text{gen}}(y)$, let $\partial_y \mathcal{E}_{\text{gen}}(y) = 0$, the intersection point of defect extremal surface and the brane is located at

$$y = u, \quad (6.5)$$

which means that the extremal surface is the same as the RT surface. This is expected because $\mathcal{E}_{\text{defect}}$ coming from brane matter is a constant. The resulting entanglement negativity from DES is

$$\mathcal{E}_{\text{DES}} = \frac{c}{4} \log \frac{2u}{\epsilon_u} + \frac{c}{4} \operatorname{arctanh}(\sin \theta_0) + \frac{c'}{4} \log \frac{2l}{\epsilon_y \cos \theta_0} . \quad (6.6)$$

6.2.2 Island result

Here we switch to the 2d gravity description. Since we have already proposed the island formula of the entanglement negativity (3.8), we will calculate it explicitly below.

In this case, it can be viewed as a single interval with length $u+y$. From the calculation in [46], we can see that

$$\mathcal{E}_{\text{eff}}(x_1, x_2) = \frac{c}{4} \log \left(\frac{|x_1 - x_2|^{2l}}{\epsilon_1 \epsilon_2 \Omega(x_1, \bar{x}_1) \Omega(x_2, \bar{x}_2)} \right) , \quad (6.7)$$

where $\epsilon_{1,2}$ are the UV cut-offs and Ω comes from the Weyl factor of the metric $ds^2 = \Omega^{-2} dx d\bar{x}$. Thus we derive the effective negativity

$$\mathcal{E}_{\text{eff}} = \frac{c}{4} \log \frac{(u+y)^{2l}}{\epsilon_u \epsilon_y y \cos \theta_0} . \quad (6.8)$$

The generalized negativity is obtained by adding area term

$$\begin{aligned} \mathcal{E}_{\text{gen}}(y) &= \mathcal{E}_{\text{eff}}([-y, u]) + \mathcal{E}_{\text{area}}(y) \\ &= \frac{c}{4} \log \frac{(u+y)^{2l}}{\epsilon_u \epsilon_y y \cos \theta_0} + \frac{c}{4} \operatorname{arctanh}(\sin \theta_0) . \end{aligned} \quad (6.9)$$

By extremizing (6.9), we require $\partial_y \mathcal{E}_{\text{gen}}(y) = 0$, thus the quantum extremal surface is located at

$$y = u , \quad (6.10)$$

which is the same as the end point of the defect extremal surface. The entanglement negativity is

$$\begin{aligned} \mathcal{E}_{\text{QES}} &= \frac{c}{4} \log \frac{4ul}{\epsilon_u \epsilon_y \cos \theta_0} + \frac{c}{4} \operatorname{arctanh}(\sin \theta_0) \\ &= \frac{c}{4} \log \frac{2u}{\epsilon_u} + \frac{c}{4} \operatorname{arctanh}(\sin \theta_0) + \frac{c}{4} \log \frac{2l}{\epsilon_y \cos \theta_0} . \end{aligned} \quad (6.11)$$

If we consider the simple case that $c' = c$, then this result would recover our previous result (6.6). The bulk defect extremal surface result agrees with the quantum extremal surface result from island formula.

6.3 Single interval $[u_1, u_2]$

6.3.1 DES result

Here we consider a general single interval (which does not contain the boundary point). In this case the entanglement negativity has a phase transition due to the variation of the cross-ratio between the operators. Note that the "phase" below always refers to the phase of the BCFT on the rigid AdS boundary.

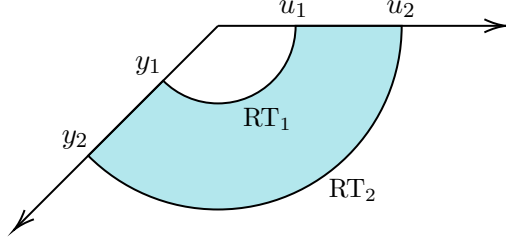


Figure 6: The disconnected phase of a single interval $[u_1, u_2]$. Disconnected phase means that the RT surface intersects with the brane.

Phase-I: connected phase In this phase, the extremal surface does not intersect with the brane. Thus $\mathcal{E}_{\text{defect}}$ vanishes and the generalized entanglement negativity is given by the boundary contributions only, i.e.

$$\mathcal{E}_{\text{gen}} = \frac{c}{2} \log \frac{(u_2 - u_1)}{\epsilon_u}, \quad (6.12)$$

which is a trivial single-interval result. See [8] for exact calculation.

Phase-II: disconnected phase The DES terminates on the brane as shown in fig.6 and the entanglement negativity of an interval $[-y_1, -y_2]$ on the brane contributes. The generalized negativity when the cross-ratio on the brane $\eta \rightarrow \infty$ is given by

$$\begin{aligned} \mathcal{E}_{\text{gen}}(y_1, y_2) &= \mathcal{E}_{\text{RT}_1} + \mathcal{E}_{\text{RT}_2} + \mathcal{E}_{\text{defect}} \\ &= \frac{c}{4} \left(\log \frac{y_1^2 + u_1^2 + 2y_1 u_1 \sin \theta_0}{(u_1 + y_1 \sin \theta_0) \epsilon_u} + \operatorname{arctanh} \frac{u_1^2 + 2y_1 u_1 \sin \theta_0 - y_1^2 \cos 2\theta_0}{u_1^2 + 2y_1 u_1 \sin \theta_0 + y_1^2} \right. \\ &\quad + \log \frac{y_2^2 + u_2^2 + 2y_2 u_2 \sin \theta_0}{(u_2 + y_2 \sin \theta_0) \epsilon_u} + \operatorname{arctanh} \frac{u_2^2 + 2y_2 u_2 \sin \theta_0 - y_2^2 \cos 2\theta_0}{u_2^2 + 2y_2 u_2 \sin \theta_0 + y_2^2} \\ &\quad \left. + \log \frac{l^2 (y_1 - y_2)^2}{y_1 y_2 \epsilon_y^2 \cos^2 \theta_0} \right). \end{aligned} \quad (6.13)$$

By extremizing $\mathcal{E}_{\text{gen}}(y_1, y_2)$ with respect to y_1 and y_2 , we find that $\partial_y \mathcal{E}_{\text{gen}}(y_1, y_2) < 0$ for any y_1 and y_2 . So there is no extremal surface. When $\eta \rightarrow 0$,

$$\begin{aligned} \mathcal{E}_{\text{gen}}(y_1, y_2) &= \mathcal{E}_{\text{RT}_1} + \mathcal{E}_{\text{RT}_2} + \mathcal{E}_{\text{defect}} \\ &= \frac{c}{4} \left(\log \frac{y_1^2 + u_1^2 + 2y_1 u_1 \sin \theta_0}{(u_1 + y_1 \sin \theta_0) \epsilon_u} + \operatorname{arctanh} \frac{u_1^2 + 2y_1 u_1 \sin \theta_0 - y_1^2 \cos 2\theta_0}{u_1^2 + 2y_1 u_1 \sin \theta_0 + y_1^2} \right. \\ &\quad + \log \frac{y_2^2 + u_2^2 + 2y_2 u_2 \sin \theta_0}{(u_2 + y_2 \sin \theta_0) \epsilon_u} + \operatorname{arctanh} \frac{u_2^2 + 2y_2 u_2 \sin \theta_0 - y_2^2 \cos 2\theta_0}{u_2^2 + 2y_2 u_2 \sin \theta_0 + y_2^2} \\ &\quad \left. + 2 \log \frac{2l}{\epsilon_y \cos \theta_0} \right). \end{aligned} \quad (6.14)$$

By extremizing $\mathcal{E}_{\text{gen}}(y_1, y_2)$ with respect to y_1 and y_2 , i.e. $\partial_{y_1} \mathcal{E}_{\text{gen}}(y_1, y_2) = \partial_{y_2} \mathcal{E}_{\text{gen}}(y_1, y_2) = 0$, we get the location of the intersection of defect extremal surface and the EOW brane

$$y_1 = u_1, \quad y_2 = u_2. \quad (6.15)$$

Following DES proposal we obtain

$$\mathcal{E}_{\text{DES}} = \frac{c}{4} \left(\log \frac{2u_1}{\epsilon_u} + \log \frac{2u_2}{\epsilon_u} + 2 \operatorname{arctanh}(\sin \theta_0) + 2 \log \frac{2l}{\epsilon_y \cos \theta_0} \right). \quad (6.16)$$

To summarize, the final results are

$$\mathcal{E}_{\text{DES}} = \begin{cases} \frac{c}{2} \log \frac{(u_1 - u_2)}{\epsilon_u}, & \eta \rightarrow \infty \\ \frac{c}{4} \left[\log \frac{4u_1 u_2}{\epsilon_u^2} + 2 \operatorname{arctanh}(\sin \theta_0) + 2 \log \frac{2l}{\epsilon_y \cos \theta_0} \right], & \eta \rightarrow 0. \end{cases} \quad (6.17)$$

6.3.2 Island result

Phase-I: connected phase In this case, the negativity only includes the boundary contribution

$$\mathcal{E}_{\text{QES}} = \frac{c}{2} \log \frac{(u_2 - u_1)}{\epsilon}. \quad (6.18)$$

Phase-II: disconnected phase Since the brane CFT is coupled to gravity, we should consider the contribution of the interval $[-y_1, -y_2]$ on the brane. The end points of the interval have corresponding area term which is given by

$$\mathcal{E}_{\text{area}} = 2 \times \frac{1}{4G_N^{(2)}} = \frac{c}{2} \operatorname{arctanh}(\sin \theta_0). \quad (6.19)$$

Considering the derivation of the negativity of multiple intervals at large central charge in [39, 50], the generalized negativity is given by

$$\begin{aligned} \mathcal{E}_{\text{gen}}(a, b) &= \mathcal{E}_{\text{area}} + \mathcal{E}_{\text{eff}}([-y_1, -y_2] \cup [u_1, u_2]) \\ &= \frac{c}{2} \operatorname{arctanh}(\sin \theta_0) \\ &\quad + \min \left\{ \frac{c}{4} \log \frac{(y_1 - y_2)^2 (u_1 - u_2)^2 l^2}{y_1 y_2 \epsilon_u^2 \epsilon_y^2 \cos^2 \theta_0}, \frac{c}{4} \log \frac{(u_1 + y_1)^2 (u_2 + y_2)^2 l^2}{y_1 y_2 \epsilon_u^2 \epsilon_y^2 \cos^2 \theta_0} \right\}, \end{aligned} \quad (6.20)$$

where the two terms in $\{\}$ correspond to the $\eta \rightarrow \infty$ and $\eta \rightarrow 0$ case respectively, with η the cross-ratio defined in (5.6). We note that the general analytic behavior of entanglement negativity in this case is very different from entanglement entropy [50], the critical point of η (the phase-transition point) should be determined by numerical calculation, but it will not affect our current discussion. As we have assumed the large c limit, from holographic side we can determine the critical point η_c by equating these two results.

In the minimization procedure, we can see for the first term $\partial_{y_2} \mathcal{E}_{\text{gen}}(y_1, y_2) < 0$, which means that there is no extremal point. By taking extremization of the second term, we have

$$y_1 = u_1, \quad y_2 = u_2. \quad (6.21)$$

Thus the final negativity is given by

$$\mathcal{E}_{\text{QES}} = \frac{c}{2} \operatorname{arctanh}(\sin \theta_0) + \frac{c}{4} \log \frac{16u_1 u_2 l^2}{\epsilon_u^2 \epsilon_y^2 \cos^2 \theta_0}. \quad (6.22)$$

To summarize,

$$\mathcal{E}_{\text{QES}} = \begin{cases} \frac{c}{2} \log \frac{(u_2 - u_1)}{\epsilon_u} , & \eta > \eta_c \\ \frac{c}{4} \left[\log \frac{4u_1 u_2}{\epsilon_u^2} + 2 \operatorname{arctanh}(\sin \theta_0) + 2 \log \frac{2l}{\epsilon_y \cos \theta_0} \right] , & \eta < \eta_c , \end{cases} \quad (6.23)$$

which is exactly the same as (6.17).

6.4 Adjacent intervals $[0, u_2]$ and $[u_2, v_2]$

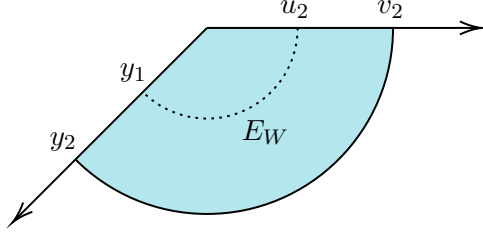


Figure 7: The case of adjacent intervals $[0, u_2]$ and $[u_2, v_2]$.

6.4.1 DES result

In this case we consider adjacent intervals on the boundary including the boundary point of BCFT, as illustrated in fig.7. Let Γ be the minimal surface in AdS_3 with two endpoints u_2 and y_1 , thus the area term is given by

$$\mathcal{E}_{\text{area}} = \frac{3}{2} \frac{\text{Area}(\Gamma)}{4G_N} = \frac{3L(y_1)}{8G_N} . \quad (6.24)$$

Now we combine the result with the calculation results from sec.5.4. For $\xi < 1$ the defect contribution is constant. Extremization of $\mathcal{E}_{\text{gen}}(y_1)$ over y_1 , i.e. letting $\partial_{y_1} \mathcal{E}_{\text{gen}}(y_1) = 0$, gives the location of the intersection point of defect extremal surface and the brane:

$$y_1 = u_2 , \quad (6.25)$$

which leads to

$$\mathcal{E}_{\text{DES}} = \text{ext}_{y_1} \{ \mathcal{E}_{\text{area}} + \mathcal{E}_{\text{defect}} \} = \frac{c}{4} \log \frac{2u_2}{\epsilon_u} + \frac{c}{4} \operatorname{arctanh}(\sin \theta_0) + \frac{c}{4} \log \frac{2l}{\epsilon_y \cos \theta_0} . \quad (6.26)$$

here we pick c' on brane equal to c . For $\xi > 1$, we have

$$\mathcal{E}_{\text{gen}} = \frac{3L(y_1)}{8G_N} + \frac{c}{4} \log \frac{2l}{\xi \epsilon_y \cos \theta_0} . \quad (6.27)$$

For (6.27), we found $\partial_{y_1} \mathcal{E}_{\text{gen}} < 0$. So there are no extremal surface and brane contributions.

6.4.2 Island result

Note that in large c limit, the four-point function factorizes. The RT surface in the outer side serves actually as an IR cut-off so it does not contribute to the negativity. When $\xi < 1$, the four-point function factorizes as

$$\langle \mathcal{T}_n(y_2) \bar{\mathcal{T}}_n^2(y_1) \mathcal{T}_n^2(u_2) \bar{\mathcal{T}}_n(v_2) \rangle = \langle \bar{\mathcal{T}}_n^2(y_1) \mathcal{T}_n^2(u_2) \rangle \langle \mathcal{T}_n(y_2) \bar{\mathcal{T}}_n(v_2) \rangle , \quad (6.28)$$

which leads to

$$\mathcal{E}_{\text{eff}} = \frac{c}{4} \log \frac{(u_2 + y_1)^2 l}{\epsilon_u \epsilon_y y_1 \cos \theta_0} . \quad (6.29)$$

The minimization gives $u_2 = y_1$, as we expected. Adding the area term and do extremization over y_1 , the generalized negativity is

$$\mathcal{E}_{\text{DES}} = \text{ext}_{y_1} \{ \mathcal{E}_{\text{area}} + \mathcal{E}_{\text{eff}} \} = \frac{c}{4} \log \frac{2u_2}{\epsilon_u} + \frac{c}{4} \text{arctanh}(\sin \theta_0) + \frac{c}{4} \log \frac{2l}{\epsilon_y \cos \theta_0} . \quad (6.30)$$

Compare (6.30) and (6.26) and we can see precise agreement.

7 Time dependent entanglement negativity in black hole evaporation

In this section we study the time dependent AdS₃/BCFT₂ setting in which an eternal black hole emerges from the boundary effective description [47, 48]. In sec.6 we have seen that the entanglement negativity calculated by the bulk DES formula agrees with that calculated by the boundary island formula. In this section we will show that in the time dependent case this agreement still holds. We also calculate the time evaluation of the entanglement negativity between different parts of the black hole system.

7.1 Review of the emergence of a 2d eternal black hole

Firstly we review how a 2d eternal black emerges from the AdS₃/BCFT₂ setting. In sec.4 we see that the bulk description of a 2d BCFT is an AdS₃ geometry with an EOW brane. The metric of the Euclidean AdS₃ bulk is given by

$$\begin{aligned} ds^2 &= \frac{l^2}{z^2} (d\tau^2 + dx^2 + dz^2) \\ &= d\rho^2 + l^2 \cosh^2 \frac{\rho}{l} \cdot \frac{d\tau^2 + dy^2}{y^2} . \end{aligned} \quad (7.1)$$

As illustrated in fig.8(a), the bulk geometry is bounded by the BCFT₂ defined on half spacetime ($\tau > 0$) and the EOW brane is located at $\tau = -z \tan \theta_0$. In Euclidean spacetime there is no difference between space and time so the choice of τ and x coordinates in fig.8(a) is just for the convenience of calculation without any physical interpretation.

In order to find a physical interpretation, we use a set of conformal transformations

$$\begin{aligned} \tau &= \frac{2(x'^2 + \tau'^2 + z'^2 - 1)}{(\tau' + 1)^2 + x'^2 + z'^2} , \\ x &= \frac{4x'}{(\tau' + 1)^2 + x'^2 + z'^2} , \\ z &= \frac{4z'}{(\tau' + 1)^2 + x'^2 + z'^2} . \end{aligned} \quad (7.2)$$

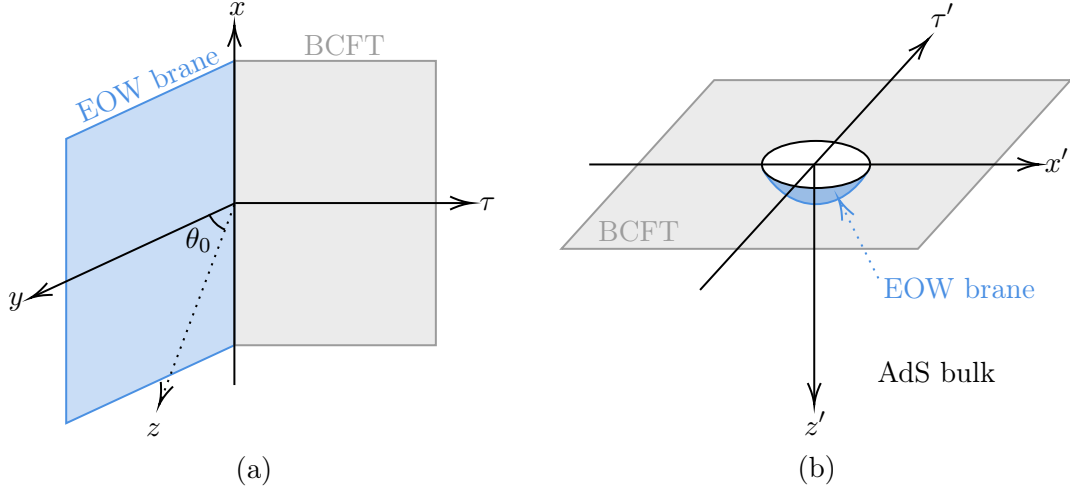


Figure 8: (a) The bulk description of the Euclidean BCFT₂. Note that here the coordinates τ and x are exchanged, which is different from the usual definition. (b) The geometry of our model after the conformal transformation (7.2). The boundary of the BCFT is mapped to a circle (7.3) and the EOW brane is mapped to a part of sphere (7.4).

As shown in fig.8(b), after this conformal transformation the boundary of the BCFT ($\tau = z = 0$) is mapped to a circle

$$x'^2 + \tau'^2 = 1, \quad (7.3)$$

and the EOW brane is mapped to a part of the sphere

$$(z' + \tan \theta_0)^2 + x'^2 + \tau'^2 = \sec^2 \theta_0, \quad (7.4)$$

while the metric is preserved

$$ds^2 = \frac{l^2}{z'^2} (d\tau'^2 + dx'^2 + dz'^2). \quad (7.5)$$

Employing the decomposition reviewed in sec.4, one can obtain a 2d effective boundary description, which is a gravitational region on the EOW brane surrounded by a bath CFT as shown in fig.8(b).

To see where is the black hole, one can analytical continue the Euclidean time to Lorentz time ($\tau' \rightarrow it'$) for the metric (7.5), as shown in fig.9. In Lorentz spacetime, the Euclidean boundary of the EOW brane (7.3) becomes $x'^2 - t'^2 = 1$. One can then introduce a coordinate system (T, X) corresponding to a Rindler observer moving along a constant-acceleration path on the right patch of this Lorentz spacetime

$$x' = e^X \cosh T, \quad t' = e^X \sinh T, \quad (7.6)$$

then the metric in this coordinate system takes the form as Rindler space, which is just the near-horizon geometry of a black hole.⁵ This procedure done in the right Rindler patch

⁵The static observers ($r = \text{constant}$) in Schwarzschild are related to constant-acceleration paths ($X = \text{constant}$) in this Rindler space.

can also be done in the left patch due to left/right \mathbb{Z}_2 symmetry. Thus, we finally obtain a 1+1 dimensional two-sided black hole coupled to a bath CFT which receives radiation emitted from the black hole.

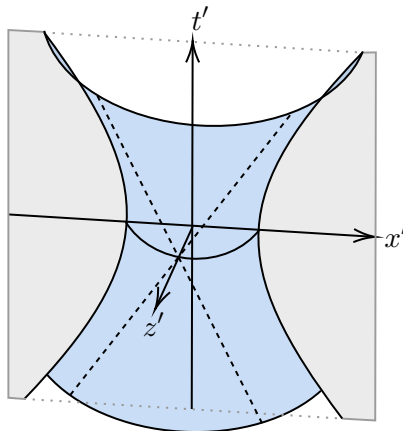


Figure 9: The Lorentz geometry of the $\text{AdS}_3/\text{BCFT}_2$ model. The gray region is the CFT bath. The blue region is the EOW brane, the boundary of which becomes hyperbolic curves in this coordinate system. The horizon on the brane is represented by black dashed lines.

The horizon of this black hole can be identified as the light-like curves on the EOW brane and its equation is given by

$$x' = \pm t' , \quad z' = \frac{1 - \sin \theta_0}{\cos \theta_0} , \quad (7.7)$$

which asymptotes to the boundary of the EOW brane $x'^2 - t'^2 = 1$ when $t' \rightarrow \infty$. The horizon is represented by the black dashed lines in fig.9.

7.2 The entanglement negativity between black hole interiors

In this section we study the entanglement negativity between black hole interiors, i.e. B_L and B_R shown in fig.10. Here we follow the setting in [47, 48] that the black hole region is defined as the space-like interval with its two endpoints at $Q(t'_0, -x'_0)$ and $P(t'_0, x'_0)$ respectively. We will first perform our calculation in Euclidean coordinates (τ, x, z) or (τ', x', z') , then analytically continue the results to Lorentz spacetime by $\tau' \rightarrow it'$ and finally use (7.6) to get the time evolution.

7.2.1 Bulk description

Phase-I: connected phase To compute $\mathcal{E}^{\text{bulk}}(B_L : B_R)$ from bulk point of view we first have to find the entanglement wedge of $B_L \cup B_R$. As shown in fig.10(a), in connected phase the extremal surface is a geodesic in AdS_3 with its two endpoints on the boundary, thus the entanglement wedge of the whole black hole is bounded by the extremal surface and a space-like interval on the boundary. The cross section connects the extremal surface (the blue arc in fig.10(a)) and the EOW brane (the dark blue region). To employ the DES formula (6.1), one has to combine the area term from the cross section with the contribution

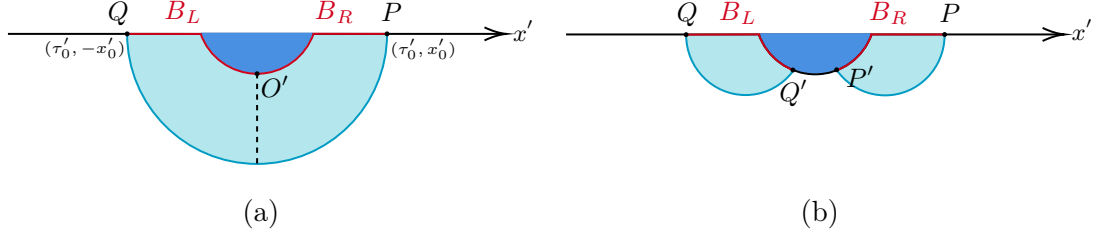


Figure 10: (a) The connected phase of the extremal surface for the black hole. (b) The disconnected phase. In this phase the two parts of the black hole are naturally separated by an island appearing in the middle. From now on we will use solid blue lines to represent the extremal surfaces, light blue regions for entanglement wedges, dark blue regions for branes, dashed lines for entanglement cross sections E_W , solid red lines for black hole regions and solid black lines for islands.

from defect negativity and then do extremization. The defect term in (6.1) is given by the single interval result (5.4), i.e.

$$\mathcal{E}_{\text{defect}}(B_L : B_R) = \frac{c}{4} \log \frac{2l}{\epsilon_y \cos \theta_0}, \quad (7.8)$$

which is a constant so we only need to extremize the area term. The calculation of the minimal cross section is similar to eq.(5.20) in [47], which gives

$$\begin{aligned} \text{Area}(\Gamma) &= l \left[\log \frac{\tau_0 + \sqrt{x_0^2 + \tau_0^2}}{x_0} + \log \frac{\cos \theta_0}{1 - \sin \theta_0} \right] \\ &= l \left[\log \frac{x_0'^2 + \tau_0'^2 - 1 + \sqrt{4x_0'^2 + (\tau_0'^2 + x_0'^2 - 1)^2}}{2x_0'} + \log \frac{\cos \theta_0}{1 - \sin \theta_0} \right]. \end{aligned} \quad (7.9)$$

Finally the entanglement negativity between B_L and B_R in the connected phase is given by

$$\mathcal{E}_{\text{conn}}^{\text{bulk}}(B_L : B_R) = \frac{c}{4} \left[\log \frac{x_0'^2 + \tau_0'^2 - 1 + \sqrt{4x_0'^2 + (\tau_0'^2 + x_0'^2 - 1)^2}}{2x_0'} + \log \frac{\cos \theta_0}{1 - \sin \theta_0} + \log \frac{2l}{\epsilon_y \cos \theta_0} \right]. \quad (7.10)$$

Phase-II: disconnected phase As shown in fig.10(b), in the disconnected phase the entanglement wedge of radiation extends to the EOW brane and this region corresponds to an island. The island splits the black hole into two parts thus the entanglement wedge of these two parts are separated, and then the area term in (6.1) vanishes. The contribution from defect is given by

$$\begin{aligned} \mathcal{E}_{\text{defect}} &= \lim_{n \rightarrow 1} \log \Omega_{Q'}^{2h_n} \Omega_{P'}^{2h_n} \langle \mathcal{T}_n(Q') \mathcal{T}_n(P') \rangle_{\text{flat}} \\ &= \lim_{n \rightarrow 1} \left| \frac{y_{Q'} \cos \theta_0}{l} \right|^{2h_n} \left| \frac{y_{P'} \cos \theta_0}{l} \right|^{2h_n} \log \langle \mathcal{T}_n(Q') \mathcal{T}_n(P') \rangle_{\text{flat}}. \end{aligned} \quad (7.11)$$

By using the doubling trick one can express the two-point correlation function on BCFT as a chiral CFT four-point correlation function on the whole plane⁶

$$\langle \mathcal{T}_n(Q') \mathcal{T}_n(P') \rangle_{\text{flat}} = \langle \mathcal{T}'_n(Q') \mathcal{T}'_n(P') \mathcal{T}'_n(P'') \mathcal{T}'_n(Q'') \rangle, \quad (7.12)$$

where $P''(y = -\tau_0, x = x_0)$ and $Q''(-\tau_0, -x_0)$ are the mirror images of P' and Q' with respect to the plane $\tau = 0$. Assuming the large c limit, then the correlator is factorized into contractions

$$\langle \mathcal{T}'_n(Q') \mathcal{T}'_n(P') \mathcal{T}'_n(P'') \mathcal{T}'_n(Q'') \rangle = \langle \mathcal{T}'_n(P') \mathcal{T}'_n(P'') \rangle \langle \mathcal{T}'_n(Q') \mathcal{T}'_n(Q'') \rangle. \quad (7.13)$$

The two-point function is given by

$$\langle \mathcal{T}'_n(P') \mathcal{T}'_n(P'') \rangle = \lim_{n \rightarrow 1} d_n |P' P''|^{-4h_n/2} = 1, \quad (7.14)$$

and note that the power is halved due to the chiral operators. Thus the defect term vanishes in this case. Finally the entanglement negativity between B_L and B_R in the disconnected phase is given by

$$\mathcal{E}_{\text{disconn}}^{\text{bulk}}(B_L : B_R) = 0. \quad (7.15)$$

7.2.2 Boundary description

Phase-I: connected phase The contribution from the matter term is given by the three-point correlator

$$\begin{aligned} \mathcal{E}_{\text{eff}}(B_L : B_R) &= \lim_{n \rightarrow 1} \log \Omega_{O'}^{2h'_n} \langle \mathcal{T}_n(Q) \bar{\mathcal{T}}_n^2(O') \mathcal{T}_n(P) \rangle \\ &= \lim_{n \rightarrow 1} \log \Omega_{O'}^{2h'_n} C_{\mathcal{T} \bar{\mathcal{T}}^2 \mathcal{T}}^n |O' Q|^{-2h'_n} |O' P|^{-2h'_n} |QP|^{2h'_n - 4h_n} \epsilon_y^{2h'_n}, \end{aligned} \quad (7.16)$$

Inserting $|O' Q| = |O' P| = \sqrt{(\tau_0 + y)^2 + x_0^2}$ and $|QP| = 2x_0$ into (7.16) and combining the area term, one gets

$$\mathcal{E}_{\text{gen}}^{\text{bdy}}(B_L : B_R) = \frac{c}{4} \left[\log \frac{l}{y \cos \theta_0} + \log 2 + \log \frac{x_0^2 + (\tau_0 + y)^2}{2x_0 \epsilon_y} + \text{arctanh}(\sin \theta_0) \right]. \quad (7.17)$$

Extremizing (7.17) over the position y gives $y = \sqrt{x_0^2 + \tau_0^2}$, thus the finally entanglement negativity is

$$\mathcal{E}_{\text{conn}}^{\text{bdy}}(B_L : B_R) = \frac{c}{4} \left[\log \frac{\tau_0 + \sqrt{\tau_0^2 + x_0^2}}{x_0} + \log \frac{2l}{\epsilon_y \cos \theta_0} + \text{arctanh}(\sin \theta_0) \right], \quad (7.18)$$

which agrees with (7.10).

⁶We use \mathcal{T}' and $\bar{\mathcal{T}}'$ to represent the chiral operators, which have half the conformal weight of the original operators.

Phase-II: disconnected phase In the disconnected phase the two parts of black hole do not intersect as shown in fig.10(b), thus in the boundary calculation there is no area term contribution and we only need to consider the matter term, which is given by the four-point correlation function

$$\mathcal{E}_{\text{gen}}^{\text{bdy}}(B_L : B_R) = \mathcal{E}_{\text{eff}}(B_L : B_R) = \lim_{n \rightarrow 1} \log \Omega_{Q'}^{2h_n} \Omega_{P'}^{2h_n} \langle \mathcal{T}_n(Q) \bar{\mathcal{T}}_n(Q') \bar{\mathcal{T}}_n(P') \mathcal{T}_n(P) \rangle . \quad (7.19)$$

As implied by the disconnected extremal surface illustrated in fig.10(b), assuming large c limit, this four-point correction function factorizes into two two-point functions

$$\langle \mathcal{T}_n(Q) \bar{\mathcal{T}}_n(Q') \bar{\mathcal{T}}_n(P') \mathcal{T}_n(P) \rangle = \langle \mathcal{T}_n(Q) \bar{\mathcal{T}}_n(Q') \rangle \langle \bar{\mathcal{T}}_n(P') \mathcal{T}_n(P) \rangle = 1 . \quad (7.20)$$

Thus in this phase the boundary result is

$$\mathcal{E}_{\text{disconn}}^{\text{bdy}}(B_L : B_R) = 0 , \quad (7.21)$$

which is consistent with the bulk calculation.

7.2.3 Time evolution

Here we rewrite the results of $\mathcal{E}(B_L : B_R)$ in the Rindler coordinates (T, X)

$$\mathcal{E}(B_L : B_R) = \begin{cases} \frac{c}{4} \left[\log \frac{e^{2X_0} - 1 + \sqrt{4e^{2X_0} \cosh^2 T + (e^{2X_0} - 1)^2}}{2e^{X_0} \cosh T} + \log \frac{\cos \theta_0}{1 - \sin \theta_0} + \log \frac{2l}{\epsilon_y \cos \theta_0} \right], & T < T_P \\ 0, & T > T_P , \end{cases} \quad (7.22)$$

where X_0 is a fixed constant specifying the boundary of the black hole region for a constant T slice in Rindler coordinates and T_P is the Page time, which is given by [48]

$$T_P = \text{arccosh} \left(\sinh X_0 e^{\text{arctanh}(\sin \theta_0)} \frac{2l}{\epsilon_y \cos \theta_0} \right) . \quad (7.23)$$

In fig.11 the time evaluation of the entanglement negativity between black hole interiors is plotted under specific parameters. The BH-BH entanglement negativity decreases at first and shifts to zero at Page time. Note that it follows the same curve of the BH-BH reflected entropy (fig.13 in [47]) up to a 3/4 factor.

7.3 The entanglement negativity between radiation and black hole

In this section we compute the entanglement negativity between radiation and black hole in the left system. Here the left part radiation refers to the semi-infinite interval $|AQ|$ as illustrated in fig.12.

7.3.1 Bulk description

Phase-I: connected phase As shown in fig.12(a), the entanglement wedge of $R_L \cup B_L$ is bounded by the boundary and associated extremal surface, which is a geodesic connects infinity to the intersection point of B_L and B_R ($x' = 0$) for the connected phase. In the connected phase the entanglement wedge cross section does not intersect with the brane,

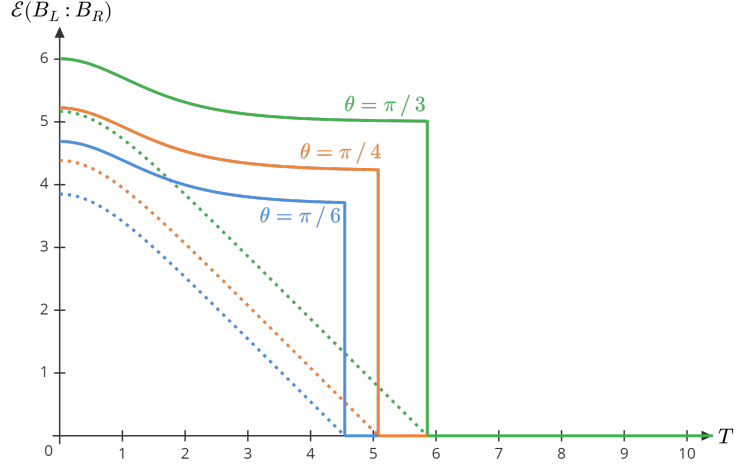


Figure 11: The entanglement negativity between black hole interiors (in the unit of $\frac{c}{4}$) with respect to time T for $X_0 = 1$ and $\theta = \frac{\pi}{6}, \frac{\pi}{4}, \frac{\pi}{3}$. We pick $\epsilon_y = 0.1$ and $l = 1$. The dash lines refer to $\frac{3}{4}$ mutual information, which decreases to zero at the Page time.

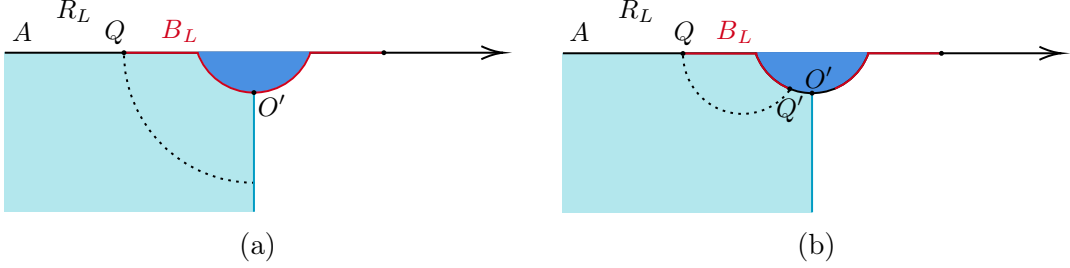


Figure 12: (a) The connected phase. (b) The disconnected phase.

thus $\mathcal{E}_{\text{defect}}$ vanishes and the generalized entanglement negativity is given by $\mathcal{E}_{\text{area}}$ only. Due to left/right \mathbb{Z}_2 symmetry, the minimal cross section between R_L and B_L is half of the extremal surface for the entire black hole $B_L \cup B_R$, which is given by eq.(3.6) in [48]. Finally the entanglement negativity between left radiation and left black hole in the connected phase is given by

$$\mathcal{E}_{\text{conn}}^{\text{bulk}}(R_L : B_L) = \frac{c}{4} \log \frac{2x'_0}{\epsilon}. \quad (7.24)$$

Phase-II: disconnected phase In the disconnected phase the cross section intersects with the EOW brane and an island of the left part radiation appears as shown in fig.12(b). To calculate the entanglement negativity in this case we have to take into account the contribution from the defect, which is given by the adjacent intervals result (5.20)

$$\mathcal{E}_{\text{defect}}(B_L : I_L) = \frac{c}{4} \log \frac{2l}{\epsilon_y \cos \theta} \quad (7.25)$$

at large c limit. The calculation of the minimal cross section is similar to eq.(3.7) in [48]. Add them together and do extremization, and one gets the entanglement negativity between

R_L and B_L in the disconnected phase

$$\begin{aligned}\mathcal{E}_{\text{disconn}}^{\text{bulk}}(R_L : B_L) &= \min_{\Gamma, X} \{ \text{ext}_{\Gamma, X} [\mathcal{E}_{\text{area}}(B_L : I_L) + \mathcal{E}_{\text{defect}}(B_L : I_L)] \} \\ &= \frac{c}{4} \left(\log \frac{x_0'^2 + \tau_0'^2 - 1}{\epsilon} + \text{arctanh}(\sin \theta_0) + \log \frac{2l}{\epsilon_y \cos \theta_0} \right) .\end{aligned}\quad (7.26)$$

7.3.2 Boundary description

Phase-I: connected phase The matter term in the connected phase is given by the entanglement negativity between the intervals $|AQ|$ and $|QO'|$, which can be computed by the BCFT two-point correlation function

$$\mathcal{E}_{\text{eff}} = \lim_{n \rightarrow 1} \log \langle \mathcal{T}_n(A) \bar{\mathcal{T}}_n^2(Q) \rangle_{\text{flat}} . \quad (7.27)$$

Since the point A is at infinity ($x'_A = -\infty$), $\mathcal{T}_n(A)$ is an identity operator. In the connected phase the cross section does not terminate on the brane thus there is no area term. Using (5.2), the entanglement negativity reads

$$\mathcal{E}_{\text{gen}}^{\text{bdy}}(R_L : B_L) = \lim_{n \rightarrow 1} \log \langle \bar{\mathcal{T}}_n^2(Q) \rangle_{\text{flat}} = \frac{c}{4} \log \frac{2x_0'}{\epsilon} , \quad (7.28)$$

which coincides with the bulk result (7.24) exactly.

Phase-II: disconnected phase In the disconnected phase the left side radiation has an entanglement island $I_L = |Q'O'|$ as illustrated in fig.12(b), thus the matter term in QES formula is the entanglement negativity between the left side radiation plus its island and the left side black hole, which reads

$$\mathcal{E}_{\text{mat}}(R_L \cup I_L : B_L) = \lim_{n \rightarrow 1} \log \Omega_{Q'}^{2h'_n} \Omega_{O'}^{2h_n} \langle \mathcal{T}_n(A) \bar{\mathcal{T}}_n^2(Q) \mathcal{T}_n^2(Q') \bar{\mathcal{T}}_n(O') \rangle . \quad (7.29)$$

At large c limit, the four-point correlator factorizes into two two-point correlators

$$\langle \mathcal{T}_n(A) \bar{\mathcal{T}}_n^2(Q) \mathcal{T}_n^2(Q') \bar{\mathcal{T}}_n(O') \rangle = \langle \mathcal{T}_n(A) \bar{\mathcal{T}}_n(O') \rangle \langle \bar{\mathcal{T}}_n^2(Q) \mathcal{T}_n^2(Q') \rangle . \quad (7.30)$$

We assume that in the (τ, x, z) coordinates Q' is located at $(-y \sin \theta_0, x, y \cos \theta_0)$, then using (5.7) one obtain

$$\begin{aligned}\mathcal{E}_{\text{gen}}^{\text{bdy}}(R_L : B_L) &= \frac{c}{4} \text{arctanh}(\sin \theta_0) + \frac{c}{4} \log \frac{l}{y \cos \theta_0} \\ &+ \frac{c}{4} \left[\log \frac{\sqrt{(\tau_0 + y)^2 + (x_0 - x)^2}}{\epsilon_y} - \log \frac{4\epsilon}{(\tau_0' + 1)^2 + x_0'^2} \right] .\end{aligned}\quad (7.31)$$

Extremizing the generalized entanglement negativity over x and y gives the position of Q' : $y = \tau_0$, $x = x_0$. Finally the Rad-BH entanglement negativity in the disconnected phase is given by

$$\begin{aligned}\mathcal{E}_{\text{disconn}}^{\text{bdy}}(R_L : B_L) &= \frac{c}{4} \left[\text{arctanh}(\sin \theta_0) + \log \frac{l}{\tau_0 \cos \theta_0} + \log \frac{4\tau_0^2}{\epsilon_y} - \log \frac{4\epsilon}{(\tau_0' + 1)^2 + x_0'^2} \right] \\ &= \frac{c}{4} \left[\text{arctanh}(\sin \theta_0) + \log \frac{2l}{\epsilon_y \cos \theta_0} + \log \frac{x_0'^2 + \tau_0'^2 - 1}{\epsilon} \right] ,\end{aligned}\quad (7.32)$$

which agrees with (7.26) exactly.

7.3.3 Time evolution

Combining (7.24) and (7.26), one can rewrite the entanglement negativity between radiation and black hole in Rindler coordinates (T, X) using (7.6)

$$\mathcal{E}(R_L : B_L) = \begin{cases} \frac{c}{4} \left(\log \frac{2 \cosh T}{\epsilon} + X_0 \right), & T < T_P \\ \frac{c}{4} \left(\log \frac{e^{2X_0} - 1}{\epsilon} + \operatorname{arctanh}(\sin \theta_0) + \log \frac{2l}{\epsilon_y \cos \theta} \right), & T > T_P, \end{cases} \quad (7.33)$$

where T_P is the Page time given by (7.23). In fig.13 we plot the time evaluation of the Rad-BH entanglement negativity. Note that it follows the same Page curve of the entanglement entropy of the whole black hole or radiation in [48] up to a constant factor.

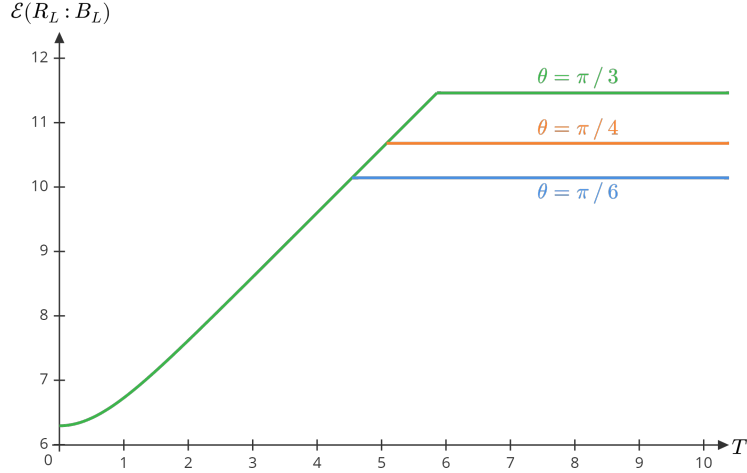


Figure 13: The entanglement negativity between radiation and black hole (in the unit of $\frac{c}{4}$) with respect to time T for $X_0 = 1$ and $\theta = \frac{\pi}{6}, \frac{\pi}{4}, \frac{\pi}{3}$. We pick $\epsilon = 0.01$, $\epsilon_y = 0.1$, and $l = 1$.

7.4 The entanglement negativity between radiation and radiation

In this section we consider the entanglement negativity between two adjacent regions of radiation, i.e. the nearby radiation and distant radiation as illustrated in fig.14 and fig.15. The nearby part radiation R_N refers to the interval $|MQ| \cup |PN|$ with its four endpoints $M(-T+i\pi, X_1)$, $Q(-T+i\pi, X_0)$, $P(T, X_0)$ and $N(T, X_1)$ in the Rindler coordinates. While the distant part R_D refers to $|EM| \cup |NF|$ with its four endpoints $E(-T+i\pi, X_2)$, M , N and $F(T, X_2)$. Similar to the previous sections, for simplicity we will first do the calculation in Euclidean spacetime. The (τ', x', z') coordinates of the endpoints are shown in fig.14(a) and they can be mapped from the (T, X) coordinates via the following transformations

$$\begin{aligned} x'_0 &= e^{X_0} \cosh T, & \tau'_0 &= ie^{X_0} \sinh T, \\ x'_1 &= e^{X_1} \cosh T, & \tau'_1 &= ie^{X_1} \sinh T, \\ x'_2 &= e^{X_2} \cosh T, & \tau'_2 &= ie^{X_2} \sinh T. \end{aligned} \quad (7.34)$$

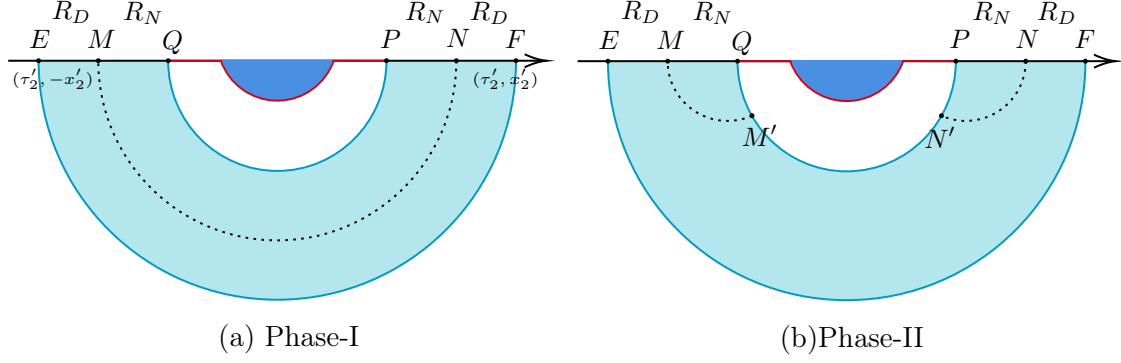


Figure 14: Possible configurations of the connected phase. (a) The entanglement wedge cross section does not terminate on the extremal surface \widehat{QP} . (b) The wedge cross sections terminate on \widehat{QP} . In this paper we do not consider the phases in which the cross section terminates on the outer extremal surface \widehat{EF} and the phases in which Q is connected to E as one can make these phases never appear by adjusting the value of X_2 to be large enough.

7.4.1 Bulk description

Phase-I As shown in Fig.14(a), the entanglement wedge of $R_N \cup R_D$ is bounded by two extremal surface. Since the conformal matter is only located on the EOW brane, there is no matter contribution within the wedge so we only need to compute the area of the cross section that separates R_N and R_D , i.e. the length of the dashed curve in fig.14(a), so we get

$$\mathcal{E}_I^{\text{bulk}}(R_N : R_D) = \frac{c}{2} \log \frac{2x'_1}{\epsilon}. \quad (7.35)$$

Phase-II From bulk description we need to calculate the extremal length of the geodesic $E_W(R_N : R_D)$ in fig.14(b). For a geodesic connected $N(\tau'_1, x'_1)$ and a point N' on the extremal surface $\widehat{QP} : x'^2 + z'^2 = x_0'^2$ & $\tau' = \tau'_0$, the length formula is given in appendix B and we denote this length by L_2

$$L_2 = \log \frac{\sqrt{[(\tau'_0 - \tau'_1)^2 + x_0'^2 + x_1'^2]^2 - 4x_0'^2 x_1'^2}}{\epsilon x'_0}. \quad (7.36)$$

Then the entanglement negativity of phase-II from the bulk description is given by

$$\mathcal{E}_{II}^{\text{bulk}}(R_N : R_D) = \frac{c}{2} \log \frac{\sqrt{[(\tau'_0 - \tau'_1)^2 + x_0'^2 + x_1'^2]^2 - 4x_0'^2 x_1'^2}}{\epsilon x'_0}. \quad (7.37)$$

Phase-III As shown in fig.15(a), an island appears in phase-III. However, the entire island belongs to R_N so the term $\mathcal{E}_{\text{defect}}(I_N : I_D = \emptyset)$ in DES formula vanishes and we just need to compute the area of entanglement wedge cross section. Obviously the entanglement wedge cross section in phase-III is the same as that in phase-I so we just get the same result

$$\mathcal{E}_{III}^{\text{bulk}}(R_N : R_D) = \frac{c}{2} \log \frac{2x'_1}{\epsilon}. \quad (7.38)$$

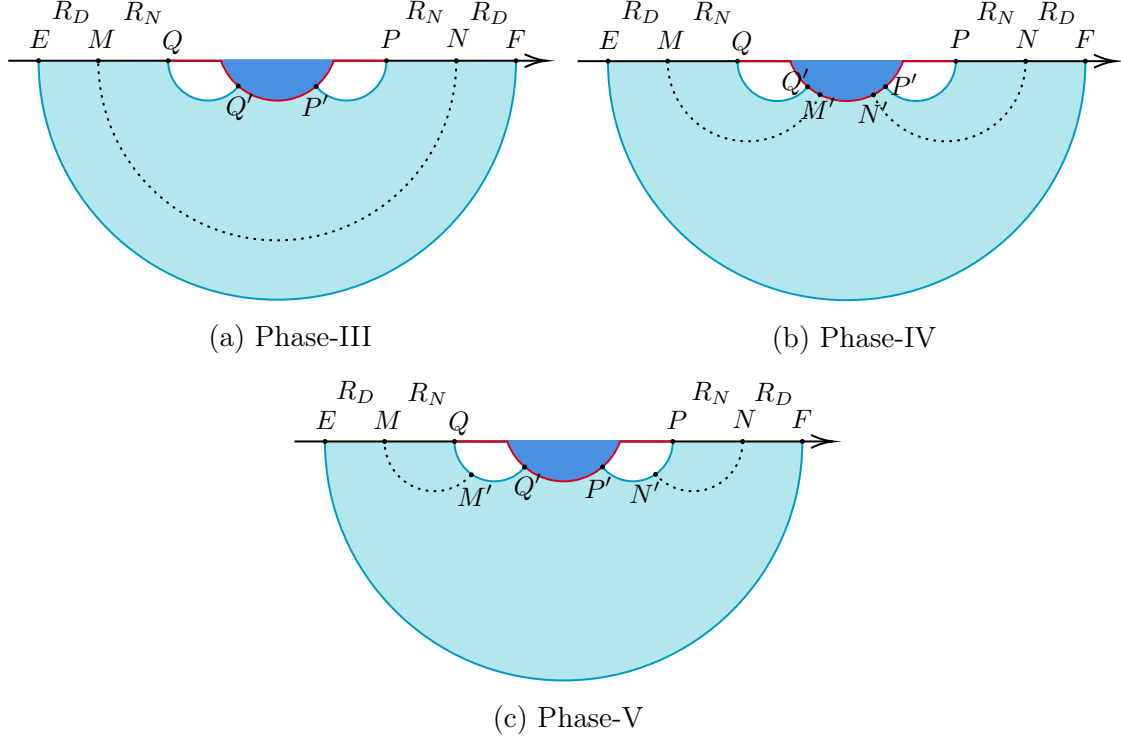


Figure 15: Possible configurations of the disconnected phase. (a) The entanglement wedge cross section does not terminate on the extremal surface \widehat{QP} . (b) The wedge cross sections terminate on the brane. (c) The wedge cross sections terminate on the extremal surface $\widehat{QQ'} \cup \widehat{P'P}$.

Phase-IV In this phase the entanglement cross sections intersect with the brane at two points M' and N' as shown in fig.15(b). By the symmetry with respect to the $x' = 0$ plane, the locations of the two intersection points M' and N' can be denoted as $(\tau'_1, \mp x'_1, z'_1)$, or $(-z'_1 \tan \theta, \mp x'_1, z'_1)$ in the coordinate system (τ, x, z) . The calculation of the extremal surface is similar to eq.(3.7) in [48], which gives

$$\begin{aligned}
\widehat{MM'}/l &= \widehat{NN'}/l \\
&= \log \frac{(\tau_1 + z_1 \tan \theta_0)^2 + (x_1 - x_1')^2 + z_1'^2}{\sqrt{(\tau_1 + z_1 \tan \theta_0)^2 + (x_1 - x_1')^2}} \\
&\quad + \operatorname{arctanh} \frac{(\tau_1 + z_1 \tan \theta_0)^2 + (x_1 - x_1')^2 - z_1'^2}{(\tau_1 + z_1 \tan \theta_0)^2 + (x_1 - x_1')^2 + z_1'^2} \\
&\quad - \log \frac{4\epsilon}{(\tau'_1 + 1)^2 + x_1'^2},
\end{aligned} \tag{7.39}$$

where the last term corresponds to the cut-off in the (τ, x, z) coordinates. The defect contribution from the negativity between $Q'M' \cup P'N'$ and $M'N'$ is given by

$$\begin{aligned}
& \mathcal{E}_{\text{defect}}(Q'M' \cup P'N' : M'N') \\
&= \lim_{n \rightarrow 1} \log \Omega_{Q'}^{2h_n} \Omega_{M'}^{2h_n} \Omega_{N'}^{2h_n} \Omega_{P'}^{2h_n} \langle \mathcal{T}_n(Q') \bar{\mathcal{T}}_n^2(M') \mathcal{T}_n^2(N') \bar{\mathcal{T}}_n(P') \rangle_{\text{flat}} \\
&= \lim_{n \rightarrow 1} \log \Omega_{M'}^{2h_n} \Omega_{N'}^{2h_n} \langle \mathcal{T}'_n(Q') \mathcal{T}'_n(Q'') \bar{\mathcal{T}}_n'^2(M') \bar{\mathcal{T}}_n'^2(M'') \mathcal{T}_n'^2(N') \mathcal{T}_n'^2(N'') \bar{\mathcal{T}}_n'(P') \bar{\mathcal{T}}_n'(P'') \rangle \\
&= \lim_{n \rightarrow 1} \log \Omega_{M'}^{2h_n} \Omega_{N'}^{2h_n} \langle \mathcal{T}'_n(Q') \mathcal{T}'_n(Q'') \rangle \langle \bar{\mathcal{T}}_n'^2(M') \bar{\mathcal{T}}_n'^2(M'') \rangle \langle \mathcal{T}_n'^2(N') \mathcal{T}_n'^2(N'') \rangle \langle \bar{\mathcal{T}}_n'(P') \bar{\mathcal{T}}_n'(P'') \rangle \\
&= \lim_{n \rightarrow 1} \log \Omega_{M'}^{2h_n} \Omega_{N'}^{2h_n} \langle \bar{\mathcal{T}}_n^2(M') \rangle_{\text{flat}} \langle \mathcal{T}_n^2(N') \rangle_{\text{flat}} .
\end{aligned} \tag{7.40}$$

In the third line, we use doubling trick. In the fourth line, the eight-point correlator is factorized into contractions assuming the large c limit. In the last line we reverse the doubling trick. Using (5.4) we get

$$\mathcal{E}_{\text{defect}}(Q'M' \cup P'N' : M'N') = \frac{c}{2} \log \frac{2l}{\epsilon_y \cos \theta_0} . \tag{7.41}$$

Note that $\mathcal{E}_{\text{defect}}(Q'M' \cup P'N' : M'N')$ is a constant so it does not shift the position of the entanglement cross section. Add the area term and the effective matter term, do extremization and we find the extremal solution is at $(-z_{1'} \tan \theta_0, \mp x_{1'}, z_{1'}) = (-\tau_1 \sin \theta, \mp x_1, \tau_1 \cos \theta_0)$. To summarize, the final entanglement negativity calculated from DES in phase-IV turns out to be

$$\mathcal{E}_{\text{IV}}^{\text{bulk}}(R_N : R_D) = \frac{c}{2} \left[\log \frac{x_1'^2 + \tau_1'^2 - 1}{\epsilon} + \text{arctanh}(\sin \theta_0) + \log \frac{2l}{\epsilon_y \cos \theta_0} \right] . \tag{7.42}$$

Phase-V First we calculate the extremal length of the geodesic $E_W(R_N : R_D)$ in fig.15(c). For a geodesic connecting $N(\tau_1', x_1')$ and a point N' on the extremal surface PP' , the length formula is given in appendix C, which we denote by L_5

$$L_5 = l \log \frac{2\sqrt{[(\tau_0' - \tau_1')^2 + (x_0' - x_1')^2] [(\tau_0'\tau_1' - 1)^2 + (x_0'x_1' - 1)^2 + \tau_0'^2 x_1'^2 + \tau_1'^2 x_0'^2 - 1]}}{\epsilon(-1 + \tau_0'^2 + x_0'^2)} . \tag{7.43}$$

Then the entanglement negativity of phase-V from the bulk description is given by

$$\mathcal{E}_{\text{V}}^{\text{bulk}}(R_N : R_D) = \frac{c}{2} \log \frac{2\sqrt{[(\tau_0' - \tau_1')^2 + (x_0' - x_1')^2] [(\tau_0'\tau_1' - 1)^2 + (x_0'x_1' - 1)^2 + \tau_0'^2 x_1'^2 + \tau_1'^2 x_0'^2 - 1]}}{\epsilon(-1 + \tau_0'^2 + x_0'^2)} . \tag{7.44}$$

7.4.2 Boundary description

Phase-I For phase-I shown in fig.14(a), the island is an empty set so we only need to compute the negativity between two adjacent intervals on a flat CFT, which can be calculated by

$$\begin{aligned}
\mathcal{E}_{\text{I}}^{\text{bdy}}(R_N : R_D) &= \mathcal{E}_{\text{eff}}(R_N : R_D) \\
&= \lim_{n \rightarrow 1} \log \langle \mathcal{T}_n(E) \bar{\mathcal{T}}_n^2(M) \mathcal{T}_n(Q) \mathcal{T}_n(P) \bar{\mathcal{T}}_n^2(N) \mathcal{T}_n(F) \rangle \\
&= \lim_{n \rightarrow 1} \log \langle \mathcal{T}_n(E) \mathcal{T}_n(F) \rangle \langle \bar{\mathcal{T}}_n^2(M) \bar{\mathcal{T}}_n^2(N) \rangle \langle \mathcal{T}_n(Q) \mathcal{T}_n(P) \bar{\mathcal{T}}_n^2(N) \rangle ,
\end{aligned} \tag{7.45}$$

where in the second line we let the correlator factorizes into its respective contractions assuming large c limit. Using (5.7) one gets

$$\mathcal{E}_I^{\text{bdy}}(R_N : R_D) = \frac{c}{2} \log \frac{2x'_1}{\epsilon} . \quad (7.46)$$

One can see that (7.46) agrees with (7.35) exactly.

Phase-II In phase-II the island is empty set so we only needs to compute $\mathcal{E}_{\text{eff}}(R_N : R_D)$

$$\begin{aligned} \mathcal{E}_{\text{II}}^{\text{bdy}}(R_N : R_D) &= \mathcal{E}_{\text{eff}}(R_N : R_D) \\ &= \lim_{n \rightarrow 1} \log \langle \mathcal{T}_n(E) \bar{\mathcal{T}}_n^2(M) \mathcal{T}_n(Q) \mathcal{T}_n(P) \bar{\mathcal{T}}_n^2(N) \mathcal{T}_n(F) \rangle \\ &= \lim_{n \rightarrow 1} \log \langle \mathcal{T}_n(E) \mathcal{T}_n(F) \rangle \langle \bar{\mathcal{T}}_n^2(M) \mathcal{T}_n(Q) \mathcal{T}_n(P) \bar{\mathcal{T}}_n^2(N) \rangle , \end{aligned} \quad (7.47)$$

To calculate the four-point function, we first use the doubling trick inversely

$$\langle \bar{\mathcal{T}}_n^2(M) \mathcal{T}_n(Q) \mathcal{T}_n(P) \bar{\mathcal{T}}_n^2(N) \rangle = \langle \tilde{\mathcal{T}}_n(P) \tilde{\mathcal{T}}_n^2(N) \rangle_{\text{flat}} . \quad (7.48)$$

The calculation of the two-point function $\langle \tilde{\mathcal{T}}_n(P) \tilde{\mathcal{T}}_n^2(N) \rangle_{\text{flat}}$ at large c limit has been discussed in sec.5.3 and here the case corresponds to the OPE channel, in which channel this BCFT correlator is equivalent to a three-point function on a flat CFT

$$\begin{aligned} \langle \tilde{\mathcal{T}}_n(P) \tilde{\mathcal{T}}_n^2(N) \rangle_{\text{flat}} &= \langle \tilde{\mathcal{T}}_n(P') \tilde{\mathcal{T}}_n(P) \tilde{\mathcal{T}}_n^2(N) \rangle \\ &= C_{\tilde{\mathcal{T}} \tilde{\mathcal{T}}^2 \tilde{\mathcal{T}}}^n |NP|^{-2\tilde{h}'_n} |NP'|^{-2\tilde{h}'_n} |PP'|^{2\tilde{h}'_n - 4\tilde{h}_n} \epsilon^{2\tilde{h}'_n} , \end{aligned} \quad (7.49)$$

where the conformal dimensions $\tilde{h}_n = 2h_n$, $\tilde{h}'_n = 2h_n$ and the OPE coefficient $C_{\tilde{\mathcal{T}} \tilde{\mathcal{T}}^2 \tilde{\mathcal{T}}}^n = 2^{c/2}$ due to the doubling trick. Thus we have

$$\mathcal{E}_{\text{II}}^{\text{bdy}}(R_N : R_D) = \frac{c}{2} \log \frac{\sqrt{[(\tau'_0 - \tau'_1)^2 + (x'_0 - x'_1)^2][(\tau'_0 - \tau'_1)^2 + (-x'_0 - x'_1)^2]}}{\epsilon x'_0} , \quad (7.50)$$

which exactly equals (7.37).

Phase-III For phase-III shown in fig.15(a), there is no area term from boundary description so the entanglement negativity is just given by

$$\begin{aligned} \mathcal{E}_{\text{III}}^{\text{bdy}}(R_N : R_D) &= \mathcal{E}_{\text{eff}}(R_N : R_D) \\ &= \lim_{n \rightarrow 1} \log \Omega_{Q'}^{2h_n} \Omega_{P'}^{2h_n} \langle \mathcal{T}_n(E) \bar{\mathcal{T}}_n^2(M) \mathcal{T}_n(Q) \mathcal{T}_n(Q') \bar{\mathcal{T}}_n(P') \bar{\mathcal{T}}_n(P) \mathcal{T}_n^2(N) \bar{\mathcal{T}}_n(F) \rangle \\ &= \lim_{n \rightarrow 1} \log \langle \mathcal{T}_n(E) \bar{\mathcal{T}}_n(F) \rangle \langle \bar{\mathcal{T}}_n^2(M) \mathcal{T}_n^2(N) \rangle \langle \mathcal{T}_n(Q) \mathcal{T}_n(Q') \rangle \langle \bar{\mathcal{T}}_n(P') \bar{\mathcal{T}}_n(P) \rangle \\ &= \frac{c}{2} \log \frac{2x'_1}{\epsilon} . \end{aligned} \quad (7.51)$$

One can see that (7.51) is the same as (7.38).

Phase-IV The matter term of phase-IV is given by

$$\begin{aligned}
& \mathcal{E}_{\text{eff}}(R_N : R_D) \\
&= \lim_{n \rightarrow 1} \log \Omega_{Q'}^{2h_n} \Omega_{M'}^{2h'_n} \Omega_{N'}^{2h'_n} \Omega_{P'}^{2h_n} \langle \mathcal{T}_n(E) \bar{\mathcal{T}}_n^2(M) \mathcal{T}_n(Q) \mathcal{T}_n(Q') \bar{\mathcal{T}}_n^2(M') \mathcal{T}_n^2(N') \bar{\mathcal{T}}_n(P') \bar{\mathcal{T}}_n(P) \mathcal{T}_n^2(N) \bar{\mathcal{T}}_n(F) \rangle \\
&= \lim_{n \rightarrow 1} \log \Omega_{M'}^{2h'_n} \Omega_{N'}^{2h'_n} \langle \mathcal{T}_n(E) \bar{\mathcal{T}}_n(F) \rangle \langle \bar{\mathcal{T}}_n^2(M) \bar{\mathcal{T}}_n^2(M') \rangle \langle \mathcal{T}_n(Q) \mathcal{T}_n(Q') \rangle \langle \mathcal{T}_n^2(N') \mathcal{T}_n^2(N) \rangle \langle \bar{\mathcal{T}}_n(P') \bar{\mathcal{T}}_n(P) \rangle \\
&= \lim_{n \rightarrow 1} \log \Omega_{M'}^{2h'_n} \Omega_{N'}^{2h'_n} \langle \bar{\mathcal{T}}_n^2(M) \bar{\mathcal{T}}_n^2(M') \rangle \langle \mathcal{T}_n^2(N') \mathcal{T}_n^2(N) \rangle .
\end{aligned} \tag{7.52}$$

Assuming that in the (τ, x, z) coordinates we have $M'(-y_{M'} \sin \theta, x_{M'}, y_{M'} \sin \theta)$ and $N'(-y_{N'} \sin \theta, x_{N'}, y_{N'} \sin \theta)$, then two-point correlators reads

$$\begin{aligned}
& \lim_{n \rightarrow 1} \log \Omega_{M'}^{2h'_n} \Omega_{N'}^{2h'_n} \langle \bar{\mathcal{T}}_n^2(M) \bar{\mathcal{T}}_n^2(M') \rangle \langle \mathcal{T}_n^2(N') \mathcal{T}_n^2(N) \rangle \\
&= \frac{c}{4} \log \frac{l}{y_{M'} \cos \theta_0} + \frac{c}{4} \log \frac{l}{y_{N'} \cos \theta_0} \\
&+ \frac{c}{4} \left[\log \frac{\sqrt{(\tau_1 + y_{M'})^2 + (-x_1 - x_{M'})^2}}{\epsilon_y} - \log \frac{4\epsilon}{(\tau'_1 + 1)^2 + x_1'^2} \right] \\
&+ \frac{c}{4} \left[\log \frac{\sqrt{(\tau_1 + y_{N'})^2 + (x_1 - x_{N'})^2}}{\epsilon_y} - \log \frac{4\epsilon}{(\tau'_1 + 1)^2 + x_1'^2} \right] .
\end{aligned} \tag{7.53}$$

Extremizing (7.53) over $y_{M'}$, $x_{M'}$, $y_{N'}$ and $x_{N'}$ gives

$$y_{M'} = \tau_1, \quad x_{M'} = -x_1, \quad y_{N'} = \tau_1, \quad x_{N'} = x_1. \tag{7.54}$$

Add the area term and finally we obtain the entanglement negativity

$$\mathcal{E}_{\text{IV}}^{\text{bdy}}(R_N : R_D) = \frac{c}{2} \left[\log \frac{x_1'^2 + \tau_1'^2 - 1}{\epsilon} + \text{arctanh}(\sin \theta_0) + \log \frac{2l}{\epsilon_y \cos \theta_0} \right]. \tag{7.55}$$

which agrees with (7.42) precisely.

Phase-V As illustrated in fig.15(c), there is no island cross section on the brane, so the entanglement negativity in the boundary description reduces to $\mathcal{E}_{\text{eff}}(R_N : R_D \cup I_D)$, which is given by

$$\begin{aligned}
& \mathcal{E}_{\text{eff}}(R_N : R_D \cup I_D) \\
&= \lim_{n \rightarrow 1} \log \Omega_{Q'}^{2h_n} \Omega_{P'}^{2h_n} \langle \mathcal{T}_n(E) \bar{\mathcal{T}}_n^2(M) \mathcal{T}_n(Q) \mathcal{T}_n(Q') \bar{\mathcal{T}}_n(P') \bar{\mathcal{T}}_n(P) \mathcal{T}_n^2(N) \bar{\mathcal{T}}_n(F) \rangle \\
&= \lim_{n \rightarrow 1} \log \langle \mathcal{T}_n(E) \bar{\mathcal{T}}_n(F) \rangle \langle \bar{\mathcal{T}}_n^2(M) \mathcal{T}_n(Q) \mathcal{T}_n(Q') \rangle \langle \bar{\mathcal{T}}_n(P') \bar{\mathcal{T}}_n(P) \mathcal{T}_n^2(N) \rangle .
\end{aligned} \tag{7.56}$$

By employing (5.15) one gets

$$\langle \bar{\mathcal{T}}_n^2(M) \mathcal{T}_n(Q) \mathcal{T}_n(Q') \rangle = 2^{c/4} |MQ|^{-2h'_n} |MQ'|^{-2h'_n} |QQ'|^{-4h_n + 2h'_n} \tilde{\epsilon}^{4h'_n}, \tag{7.57}$$

where $\tilde{\epsilon}$ is the UV cut-off of $(\tau_1, x_1, 0)$ in (τ, x, z) coordinates. We also have

$$\begin{aligned}
|M Q| &= \sqrt{(\tau_0 - \tau_1)^2 + (x_0 - x_1)^2}, \\
|M Q'| &= \sqrt{(\tau_0 + \tau_1)^2 + (x_0 - x_1)^2}, \\
|Q Q'| &= 2\tau_0.
\end{aligned} \tag{7.58}$$

One can compute $\langle \bar{\mathcal{T}}_n(P') \bar{\mathcal{T}}_n(P) \mathcal{T}_n^2(N) \rangle$ using the same method. Insert (7.57), (7.58) into (7.56), we get

$$\begin{aligned} \mathcal{E}_V^{\text{bdy}}(R_N : R_D) &= \frac{c}{2} \log \frac{\sqrt{[(\tau_0 - \tau_1)^2 + (x_0 - x_1)^2][(\tau_0 + \tau_1)^2 + (x_0 - x_1)^2]}}{\tilde{\epsilon} \tau_0} , \\ &= \frac{c}{2} \log \frac{2\sqrt{[(\tau'_0 - \tau'_1)^2 + (x'_0 - x'_1)^2][(\tau'_0 \tau'_1 - 1)^2 + (x'_0 x'_1 - 1)^2 + \tau_0'^2 x_1'^2 + \tau_1'^2 x_0'^2 - 1]}}{\epsilon(-1 + \tau_0'^2 + x_0'^2)} . \end{aligned} \quad (7.59)$$

One can see that (7.59) coincides with (7.44) exactly.

7.4.3 Time evolution

Here we summarize our results by transforming to the Rindler coordinate via (7.34) and we get the time evolution. Note that we also assume that $X_0 < X_1 < X_2$.

Phase-I

$$\mathcal{E}_I(R_N : R_D) = \frac{c}{2} \log \frac{2e^{X_1} \cosh T}{\epsilon} . \quad (7.60)$$

Phase-II

$$\mathcal{E}_{II}(R_N : R_D) = \frac{c}{2} \log \frac{(e^{X_1} - e^{X_0}) \sqrt{e^{2X_0} + e^{2X_1} + 2e^{X_0+X_1} \cosh 2T}}{\epsilon e^{X_0} \cosh T} . \quad (7.61)$$

Phase-III (Note that phase-III is the same as phase-I)

$$\mathcal{E}_{III}(R_N : R_D) = \frac{c}{2} \log \frac{2e^{X_1} \cosh T}{\epsilon} . \quad (7.62)$$

Phase-IV

$$\mathcal{E}_{IV}(R_N : R_D) = \frac{c}{2} \left[\log \frac{e^{2X_1} - 1}{\epsilon} + \operatorname{arctanh}(\sin \theta) + \log \frac{2l}{\epsilon_y \cos \theta} \right] . \quad (7.63)$$

Phase-V

$$\mathcal{E}_V(R_N : R_D) = \frac{c}{2} \log \frac{2(e^{X_1} - e^{X_0})(e^{X_0+X_1} - 1)}{\epsilon(e^{2X_0} - 1)} . \quad (7.64)$$

The entanglement negativity between nearby radiation and distant radiation experiences two phases. The early time phase corresponds to the connected extremal surface, where the entanglement negativity is given by the minimum value in \mathcal{E}_I and \mathcal{E}_{II} . The late time phase corresponds to the disconnected extremal surface and the negativity is the minimum value in \mathcal{E}_{III} , \mathcal{E}_{IV} and \mathcal{E}_V . In summary, the entanglement negativity between nearby radiation and distant radiation is given by

$$\mathcal{E}(R_N : R_D) = \begin{cases} \min \{ \mathcal{E}_I, \mathcal{E}_{II} \} , & T < T_P \\ \min \{ \mathcal{E}_{III}, \mathcal{E}_{IV}, \mathcal{E}_V \} , & T > T_P . \end{cases} \quad (7.65)$$

The result under specific parameters is plotted in fig.16. One can see that before Page time, phase-I and phase-II dominant. At the beginning after Page time, phase-III dominant, which gives the same result as phase-I and later it shifts to phase-V which is a constant all the time.

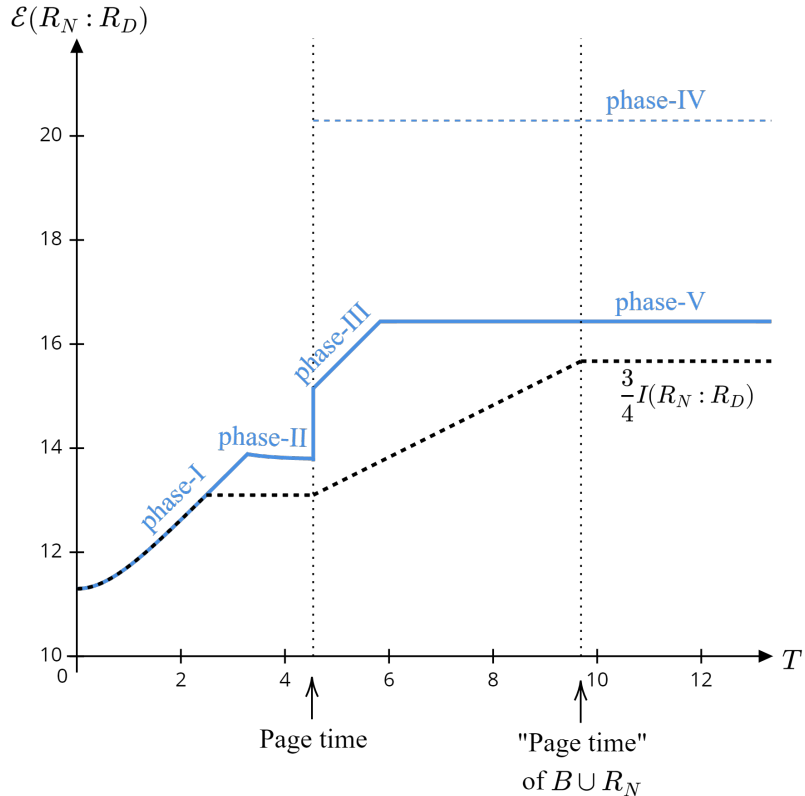


Figure 16: Time evolution of the entanglement negativity between nearby radiation and distant radiation (in the unit of $\frac{c}{2}$) with respect to time T . We set $X_0 = 1$, $X_1 = 6$, $l = 1$, $\theta = \frac{\pi}{6}$, $\epsilon = 0.01$, and $\epsilon_y = 0.1$ but note that in such a setting the final result does not rely on ϵ_y . The black dash line shows the evolution of $\frac{3}{4}I(R_N : R_D)$.

8 Conclusions and discussions

In this paper we have studied entanglement negativity for evaporating black hole based on the holographic model with defect brane. We start from the holographic dual of entanglement negativity for adjacent intervals in $\text{AdS}_3/\text{CFT}_2$ and generalize it to the island formula. To test this formula, we work in AdS_3 with a EOW brane as a bulk defect. Including the contribution from the defect theory on the brane, we propose the defect extremal surface formula for negativity. On the other hand, this model is tightly related to a lower dimensional gravity system glued to a quantum bath. In fact there is a concrete procedure, including both Randall-Sundrum and Maldacena duality, to give a lower dimensional effective description for the same system. We demonstrate the equivalence between defect extremal surface formula and island formula for negativity in $\text{AdS}_3/\text{BCFT}_2$. Extending the study to the model of eternal black hole plus CFT bath, we find that black hole-radiation negativity follows Page curve, black hole-black hole negativity decreases until vanishing, radiation-radiation negativity increases and then saturates at a time later than Page time. In all the time dependent cases, defect extremal formula agrees with island formula.

Note that there is an alternative holographic proposal for entanglement negativity in

adjacent intervals, given by mutual information multiplied by 3/4. One might naively promote 3/4 mutual information to its island formula, which is nothing but a linear combination of three island formulas for von Neumann entropy. We plotted the curves computed from the naively promoted formula, for black hole-black hole negativity and radiation-radiation negativity. We admit that so far we can not prove either one, but just remark that for general quantum system (coupled to gravity), mutual information also measures classical correlation, which is quite different from negativity. So it is unlikely that the island of mutual information can be the final formula. We leave further study on these two different proposals to future.

There are a few future questions listed in order: First, a general holographic dual for negativity. In this paper we mainly focus on the adjacent intervals and the precise holographic dual for negativity of two disjoint intervals is still open. As pointed out by Dong, Qi and Walter [53], there could be dominate contributions from replica non-symmetric saddles. How to find the general holographic dual is essentially the key to find a general island formula. Second, a CFT calculation to justify replica non-symmetric saddles. Inspired from [53], for $n = 2m$ replicas one can take Z_m quotient and there are eight-point functions left over for two disjoint intervals. Developing the CFT techniques to incorporate the replica non-symmetric saddles is crucial to understand negativity in QFT. See also [56] for related discussion. Last, compare our negativity curve to those in other models. For instance, there are recent studies of negativity in JT+EOW models of evaporating black holes [57]. It would be interesting to compare these results. We leave these to future work.

Acknowledgments

We are grateful for the useful discussions with Tianyi Li, Jinwei Chu and our group members in Fudan University. This work is supported by NSFC grant 11905033. YZ is also supported by NSFC 11947301 through Peng Huanwu Center for Fundamental Theory.

A OPE structure constant for three point function

In this appendix we give a derivation of the OPE coefficient $C_{\mathcal{T}\bar{\mathcal{T}}^2\mathcal{T}}$ by comparing the three-point function in the pure state limit with the two-point function. First we consider the following conformal transformation

$$\begin{aligned} z &= \frac{l(l^2 - r^2 + \tau^2)}{l^2 + r^2 + 2rl \cos \theta - \tau^2} , \\ x &= \frac{2l^2 r \sin \theta}{l^2 + r^2 + 2rl \cos \theta - \tau^2} , \\ t &= \frac{2l^2 \tau}{l^2 + r^2 + 2rl \cos \theta - \tau^2} . \end{aligned} \tag{A.1}$$

After this conformal transformation, the boundary of the time slice $t = 0$ in the (t, x, z) coordinates is mapped to a circle

$$\tau = 0 , \quad r = l , \quad \theta \in (-\pi, \pi] \tag{A.2}$$

while its AdS bulk is mapped to a Poincaré disk bounded by (A.2) and its metric is given by

$$ds^2 = \left(\frac{2}{1-r^2/l^2} \right)^2 (dr^2 + r^2 d\theta^2) . \quad (\text{A.3})$$

In this appendix we will always consider the boundary correlation function on this time slice, i.e. the slice with $\{t = z = 0\}$ in the (t, x, z) coordinates or $\{\tau = 0, r = l\}$ in the (τ, r, θ) coordinates. Now we consider the three-point function $\langle \mathcal{T}_n(x_1) \bar{\mathcal{T}}_n^2(0) \mathcal{T}_n(x_2) \rangle$. Using (A.1), one gets

$$x_1 = l \tan \frac{\theta_1}{2} , \quad x_2 = l \tan \frac{\theta_2}{2} . \quad (\text{A.4})$$

According to

$$\langle \mathcal{T}_n(\theta_1) \bar{\mathcal{T}}_n^2(0) \mathcal{T}_n(\theta_2) \rangle = \left| \frac{dx}{d(l\theta)} \right|_{\theta_1}^{2h_n} \left| \frac{dx}{d(l\theta)} \right|_0^{2h'_n} \left| \frac{dx}{d(l\theta)} \right|_{\theta_2}^{2h_n} \langle \mathcal{T}_n(x_1) \bar{\mathcal{T}}_n^2(0) \mathcal{T}_n(x_2) \rangle , \quad (\text{A.5})$$

one gets⁷

$$\begin{aligned} \lim_{n \rightarrow 1} \log \langle \mathcal{T}_n(\theta_1) \bar{\mathcal{T}}_n^2(0) \mathcal{T}_n(\theta_2) \rangle &= \frac{c}{4} \log \left(\left| \frac{dx}{d(l\theta)} \right|_0^{-1} \frac{-C_{\mathcal{T}\bar{\mathcal{T}}^2\mathcal{T}} x_1 x_2}{(x_2 - x_1)\epsilon} \right) \\ &= \frac{c}{4} \log \frac{-2l \tan \frac{\theta_1}{2} \tan \frac{\theta_2}{2}}{(\tan \frac{\theta_2}{2} - \tan \frac{\theta_1}{2})\epsilon} + \frac{c}{4} \log C_{\mathcal{T}\bar{\mathcal{T}}^2\mathcal{T}} . \end{aligned} \quad (\text{A.6})$$

The three-point function can be reduced to a two-point function by taking the pure state limit

$$\theta_1 = -2\pi + \theta_2 + 2\epsilon/l , \quad (\text{A.7})$$

and then one gets

$$\lim_{\epsilon \rightarrow 0^+} \lim_{n \rightarrow 1} \log \langle \mathcal{T}_n(-2\pi + \theta_2 + 2\epsilon/L) \bar{\mathcal{T}}_n^2(0) \mathcal{T}_n(\theta_2) \rangle = \frac{c}{4} \log \frac{2l^2 \sin^2 \frac{\theta_2}{2}}{\epsilon^2} + \frac{c}{4} \log C_{\mathcal{T}\bar{\mathcal{T}}^2\mathcal{T}} . \quad (\text{A.8})$$

As illustrated in fig.17, the three-point function in (A.8) corresponds to the two-point function $\langle \bar{\mathcal{T}}_n^2(0) \mathcal{T}_n^2(x_2) \rangle$ with its two cut-offs both ϵ , i.e.

$$\begin{aligned} \lim_{n \rightarrow 1} \log \langle \bar{\mathcal{T}}_n^2(0) \mathcal{T}_n^2(\theta_2) \rangle &= \lim_{n \rightarrow 1} \log \left| \frac{dx}{d(l\theta)} \right|_0^{2h'_n} \left| \frac{dx}{d(l\theta)} \right|_{\theta_2}^{2h'_n} \langle \bar{\mathcal{T}}_n^2(0) \mathcal{T}_n^2(x_2) \rangle \\ &= \frac{c}{4} \log \left(2 \cdot 2 \cos^2 \frac{\theta_2}{2} \cdot \frac{x_2^2}{\epsilon^2} \right) \\ &= \frac{c}{4} \log \frac{4l^2 \sin^2 \frac{\theta_2}{2}}{\epsilon^2} . \end{aligned} \quad (\text{A.9})$$

Comparing (A.8) and (A.9), we obtain

$$C_{\mathcal{T}\bar{\mathcal{T}}^2\mathcal{T}} = 2^{c/4} . \quad (\text{A.10})$$

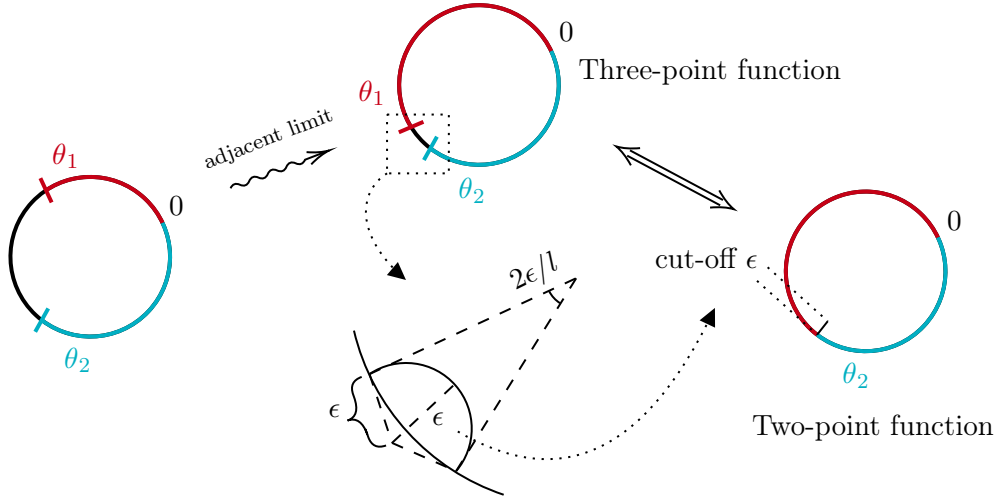


Figure 17: The correspondence between the three-point function $\langle \mathcal{T}_n(\theta_1) \bar{\mathcal{T}}_n^2(0) \mathcal{T}_n(\theta_2) \rangle$ after taking the adjacent limit (A.7) and the two-point function $\langle \bar{\mathcal{T}}_n^2(0) \mathcal{T}_n^2(\theta_2) \rangle$. The adjacent limit means that the distance between the two \mathcal{T}_n operators in the three-point function is 2ϵ , which corresponds to a UV cut-off ϵ at the same position (subfig at the bottom of the center). One can then match the three-point function after taking the limit to a two-point function with cut-off ϵ at its two endpoints.

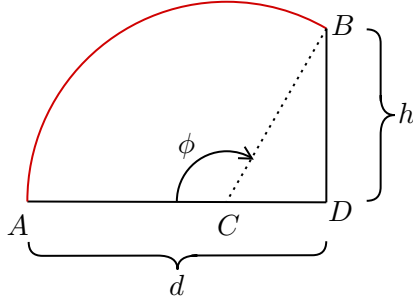


Figure 18: A slice perpendicular to the $\tau' - x'$ plane. The solid red line is the geodesic with C its center. A and B are the ending points of the geodesic, with A on the $\tau' - x'$ plane and h the z' coordinate of B . d is the distance between the projections of A and B on $\tau' - x'$ plane.

B The length formula of L_2

The computation of L_2 in the coordinates (τ', x', z') is as follow. First we derive a general expression of the length of geodesic shown in fig.18.

The radius of the geodesic R_g can be determined by $|AC| = |BC|$

$$|CD| = \frac{d^2 - h^2}{2d}, \quad R_g = |CA| = |CB| = \frac{d^2 + h^2}{2d}. \quad (\text{B.1})$$

⁷In appendix A we take the UV cut-off on the time slice $(\tau = 0, r, \theta)$ a constant, i.e. $r = L - \epsilon$.

According to the metric given by (7.5), we can compute the length of geodesic

$$L_0(d, h) = \int_{\phi=\phi_\epsilon}^{\phi_B} l \frac{R_g d\phi}{R_g \sin \phi} = \left[l \log \tan \frac{\phi}{2} \right]_{\phi=\phi_\epsilon}^{\phi_B}, \quad (\text{B.2})$$

where ϕ_B is the angle between CA and CB , ϕ_ϵ comes from the the UV cut-off $z' = \epsilon$ of the asymptotic boundary. Using (d, h, ϵ) to express (ϕ_ϵ, ϕ_B) and we get

$$L_0(d, h) = l \log \frac{d^2 + h^2}{\epsilon h}. \quad (\text{B.3})$$

Then we calculate L_2 . As shown in fig.14(b), N' can move on the extremal surface so we introduce α to parameterize the position of N' . The coordinate of N' can be represented by $(\tau', x', z') = (\tau'_0, x'_0 \sin \alpha, x'_0 \cos \alpha)$ with $\alpha \in (-\pi, \pi)$. So the length of geodesic connecting $N(\tau'_1, x'_1, 0)$ and N' is given by

$$L_0(\sqrt{(\tau'_0 - \tau'_1)^2 + (x'_0 \sin \alpha - x'_1)^2}, x'_0 \cos \alpha) = l \log \frac{(\tau'_0 - \tau'_1)^2 + (x'_0 \sin \alpha - x'_1)^2 + x_0'^2 \cos^2 \alpha}{\epsilon x'_0 \cos \alpha}, \quad (\text{B.4})$$

which is a function of α . By extremizing (B.4) with respect to α , we get (7.36) with $\sin \alpha = \frac{2x'_0 x'_1}{(\tau'_0 - \tau'_1)^2 + x_0'^2 + x_1'^2}$.

C The length formula of L_5

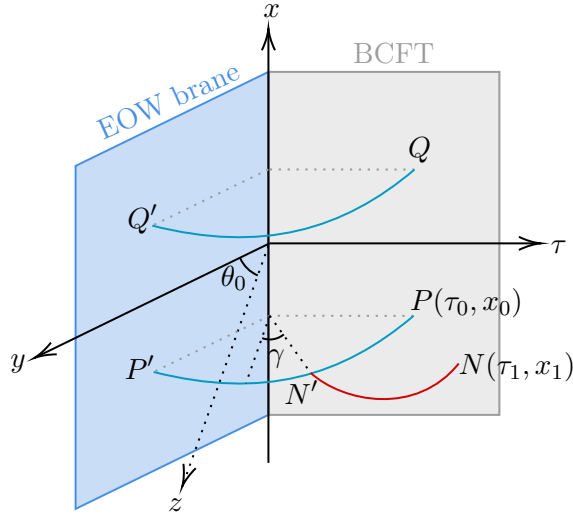


Figure 19: This figure is fig.15(c) viewed in (τ, x, z) coordinate. The RT surfaces (blue solid lines) are arcs centered on the x -axis. The entanglement wedge cross section is drawn with a solid red line.

We calculate L_5 in the coordinates (τ, x, z) as shown in fig.19. Since the expression of the metric is the same in (τ, x, z) and (τ', x', z') , we can use (B.3) to write the the length

of $\widehat{NN'}$

$$L_0(\sqrt{(\tau_0 \sin \gamma - \tau_1)^2 + (x_0 - x_1)^2}, \tau_0 \cos \gamma) = l \log \frac{(\tau_0 \sin \gamma - \tau_1)^2 + (x_0 - x_1)^2 + \tau_0^2 \cos^2 \gamma}{\tilde{\epsilon} \tau_0 \cos \gamma}, \quad (\text{C.1})$$

where γ is introduced to parameterize the position of N' , $\tilde{\epsilon}$ is the position-dependent cut-off in (τ, x, z) coordinates which is given by $\tilde{\epsilon} = \frac{4\epsilon}{(\tau_1+1)^2+x_1^2}$. Extremizing (C.1) leads to the extremal solution

$$L_5 = l \log \frac{\sqrt{[\tau_0^2 + \tau_1^2 + (x_0 - x_1)^2]^2 - 4\tau_0^2 \tau_1^2}}{\tilde{\epsilon} \tau_0}. \quad (\text{C.2})$$

We return to (τ', x', z') by coordinate transformation (7.2)

$$L_5 = l \log \frac{2\sqrt{[(\tau'_0 - \tau'_1)^2 + (x'_0 - x'_1)^2] [(\tau'_0 \tau'_1 - 1)^2 + (x'_0 x'_1 - 1)^2 + \tau_0'^2 x_1'^2 + \tau_1'^2 x_0'^2 - 1]}}{\epsilon(-1 + \tau_0'^2 + x_0'^2)}. \quad (\text{C.3})$$

References

- [1] S. Hawking, *Breakdown of Predictability in Gravitational Collapse*, *Phys. Rev. D* **14**, (1976) 2460-2473.
- [2] D. N. Page, *Information in black hole radiation*, *Phys. Rev. Lett.* **71**, (1993) 3743-3746.
- [3] D. N. Page, *Time Dependence of Hawking Radiation Entropy*, *JCAP* **09**, (2013) 028.
- [4] G. Vidal and R. F. Werner, *Computable measure of entanglement*, *Phys. Rev. A* **65**, (2002) 032314.
- [5] M. B. Plenio, *Logarithmic Negativity: A Full Entanglement Monotone That is not Convex*, *Phys. Rev. Lett.* **95** (2005) no.9, 090503 doi:10.1103/PhysRevLett.95.090503 [arXiv:quant-ph/0505071 [quant-ph]].
- [6] P. Calabrese and J. Cardy, *Entanglement entropy and quantum field theory*, *J. Stat. Mech.*, (2004) P06002.
- [7] P. Calabrese, J. Cardy and E. Tonni, *Entanglement negativity in quantum field theory*, *Phys. Rev. Lett.* **109** (2012), 130502.
- [8] P. Calabrese, J. Cardy and E. Tonni, *Entanglement negativity in extended systems: a field theoretical approach*, *J. Stat. Mech.* **02** (2013) P02008.
- [9] P. Calabrese, L. Tagliacozzo and E. Tonni, *Entanglement negativity in the critical Ising chain*, *J. Stat. Mech.* **05** (2013) P05002.
- [10] V. Alba, *Entanglement negativity and conformal field theory: a Monte Carlo study*, *J. Stat. Mech.* **1305** (2013), P05013 doi:10.1088/1742-5468/2013/05/P05013 [arXiv:1302.1110 [cond-mat.stat-mech]].
- [11] A. Coser, E. Tonni and P. Calabrese, *Entanglement negativity after a global quantum quench*, *J. Stat. Mech.* **1412** (2014) no.12, P12017 doi:10.1088/1742-5468/2014/12/P12017 [arXiv:1410.0900 [cond-mat.stat-mech]].
- [12] P. Calabrese, J. Cardy and E. Tonni, *Finite temperature entanglement negativity in conformal field theory*, *J. Phys. A* **48** (2015) no.1, 015006 doi:10.1088/1751-8113/48/1/015006 [arXiv:1408.3043 [cond-mat.stat-mech]].

- [13] M. Hoogeveen and B. Doyon, *Entanglement negativity and entropy in non-equilibrium conformal field theory*, *Nucl. Phys. B* **898** (2015), 78-112 doi:10.1016/j.nuclphysb.2015.06.021 [arXiv:1412.7568 [cond-mat.stat-mech]].
- [14] O. Blondeau-Fournier, O. A. Castro-Alvaredo and B. Doyon, *Universal scaling of the logarithmic negativity in massive quantum field theory*, *J. Phys. A* **49** (2016) no.12, 125401 doi:10.1088/1751-8113/49/12/125401 [arXiv:1508.04026 [hep-th]].
- [15] X. Wen, P. Y. Chang and S. Ryu, *Entanglement negativity after a local quantum quench in conformal field theories*, *Phys. Rev. B* **92** (2015) no.7, 075109 doi:10.1103/PhysRevB.92.075109 [arXiv:1501.00568 [cond-mat.stat-mech]].
- [16] P. Ruggiero, V. Alba and P. Calabrese, *Negativity spectrum of one-dimensional conformal field theories*, *Phys. Rev. B* **94** (2016) no.19, 195121 doi:10.1103/PhysRevB.94.195121 [arXiv:1607.02992 [cond-mat.stat-mech]].
- [17] P. Ruggiero, V. Alba and P. Calabrese, *Entanglement negativity in random spin chains*, *Phys. Rev. B* **94** (2016) no.3, 035152 doi:10.1103/PhysRevB.94.035152 [arXiv:1605.00674 [cond-mat.str-el]].
- [18] L. Capizzi, S. Murciano and P. Calabrese, *Rényi entropy and negativity for massless Dirac fermions at conformal interfaces and junctions*, [arXiv:2205.04722 [hep-th]].
- [19] V. Alba and F. Carollo, *Logarithmic negativity in out-of-equilibrium open free-fermion chains: An exactly solvable case*, [arXiv:2205.02139 [cond-mat.stat-mech]].
- [20] B. Bertini, K. Klobas and T. C. Lu, *Entanglement Negativity and Mutual Information after a Quantum Quench: Exact Link from Space-Time Duality*, [arXiv:2203.17254 [quant-ph]].
- [21] C. Castelnovo, *Negativity and topological order in the toric code*, *Physical Review A*, **88** (2013) no.4, 042319.
- [22] Y. A. Lee and G. Vidal, *Entanglement negativity and topological order*, *Physical Review A*, **88** (2013) no.4, 042318.
- [23] T. C. Lu, T. H. Hsieh and T. Grover, *Detecting Topological Order at Finite Temperature Using Entanglement Negativity*, *Phys. Rev. Lett.* **125** (2020) no.11, 116801 doi:10.1103/PhysRevLett.125.116801 [arXiv:1912.04293 [cond-mat.str-el]].
- [24] X. Wen, P. Y. Chang and S. Ryu, *Topological entanglement negativity in Chern-Simons theories*, *JHEP* **09** (2016), 012 doi:10.1007/JHEP09(2016)012 [arXiv:1606.04118 [cond-mat.str-el]].
- [25] X. Wen, S. Matsuura and S. Ryu, *Edge theory approach to topological entanglement entropy, mutual information and entanglement negativity in Chern-Simons theories*, *Phys. Rev. B* **93** (2016) no.24, 245140 doi:10.1103/PhysRevB.93.245140 [arXiv:1603.08534 [cond-mat.mes-hall]].
- [26] P. Di Francesco, P. Mathieu and D. Senechal, *Conformal Field Theory*, Springer-Verlag (1997).
- [27] J. D. Brown and M. Henneaux, *Central charges in the canonical realization of asymptotic symmetries: an example from three-dimensional gravity*, *Commun. Math. Phys.* **104**, (1986) 207-226.
- [28] A. Almheiri, N. Engelhardt, D. Marolf and H. Maxfield, *The entropy of bulk quantum fields and the entanglement wedge of an evaporating black hole*, *JHEP* **12**, (2019) 063.

- [29] A. Almheiri, R. Mahajan, J. Maldacena and Y. Zhao, *The Page curve of Hawking radiation from semiclassical geometry*, *JHEP* **03**, (2020) 149.
- [30] A. Almheiri, T. Hartman, J. Maldacena, E. Shaghoulian and A. Tajdini, *Replica Wormholes and the Entropy of Hawking Radiation*, *JHEP* **05**, (2020) 013.
- [31] G. Penington, S. H. Shenker, D. Stanford and Z. Yang, *Replica wormholes and the black hole interior*, arXiv:1911.11977.
- [32] A. Almheiri, T. Hartman, J. Maldacena, E. Shaghoulian and A. Tajdini, *The entropy of Hawking radiation*, *Rev. Mod. Phys.* **93**, (2021) 035002.
- [33] S. Ryu and T. Takayanagi, *Holographic derivation of entanglement entropy from AdS/CFT*, *Phys. Rev. Lett.* **96**, (2006) 181602.
- [34] V. E. Hubeny, M. Rangamani and T. Takayanagi, *A Covariant holographic entanglement entropy proposal*, *JHEP* **0707** (2007) 062.
- [35] H. Casini, M. Huerta and R. C. Myers, *Towards a derivation of holographic entanglement entropy*, *JHEP* **05**, (2011) 036.
- [36] A. Lewkowycz and J. Maldacena, *Generalized gravitational entropy*, *JHEP* **08**, (2013) 090.
- [37] T. Faulkner, A. Lewkowycz and J. Maldacena, *Quantum corrections to holographic entanglement entropy*, *JHEP* **11**, (2013) 074.
- [38] N. Engelhardt and A. C. Wall, *Quantum extremal surfaces: holographic entanglement entropy beyond the classical regime*, *JHEP* **01**, (2015) 073.
- [39] T. Hartman, *Entanglement Entropy at Large Central Charge*, arXiv:1303.6955.
- [40] T. Faulkner, *The Entanglement Renyi Entropies of Disjoint Intervals in AdS/CFT*, arXiv:1303.7221.
- [41] T. Takayanagi and K. Umemoto, *Entanglement of purification through holographic duality*, *Nature Phys.* **14** (2018) 6, 573-577
- [42] T. Takayanagi, *Holographic dual of BCFT*, *Phys. Rev. Lett.* **107** (2011) 101602.
- [43] X. Dong and A. Lewkowycz, *Entropy, Extremality, Euclidean Variations, and the Equations of Motion*, *JHEP* **01** (2018) 081 doi:10.1007/JHEP01(2018)081 [arXiv:1705.08453 [hep-th]].
- [44] J. Sully, M. Van Raamsdonk, and D. Wakeham, *BCFT entanglement entropy at large central charge and the black hole interior*, arxiv:2004.13088.
- [45] L. Randall and R. Sundrum, *A Large mass hierarchy from a small extra dimension*, *Phys. Rev. Lett.* **83**, (1999) 3370-3373.
- [46] F. Deng, J. Chu and Y. Zhou, *Defect extremal surface as the holographic counterpart of island*, arxiv:2012.07612.
- [47] T. Li, M.-K. Yuan, and Y. Zhou, *Defect Extremal Surface for Reflected Entropy*, arXiv:2108.08544.
- [48] J. Chu, F. Deng and Y. Zhou, *Page Curve from Defect Extremal Surface and Island in Higher Dimensions*, arXiv:2105.09106.
- [49] M. Rangamani and M. Rota, *Comments on entanglement negativity in holographic field theories*, *JHEP* **10** (2014), 060.

- [50] M. Kulaxizi, A. Parnachev and G. Policastro, *Conformal Blocks and Negativity at Large Central Charge*, *JHEP* **09**, (2014) 010.
- [51] J. Kudler-Flam and S. Ryu, *Entanglement negativity and minimal entanglement wedge cross sections in holographic theories*, *Phys. Rev. D* **99** (2019) 106014.
- [52] Y. Kusuki, J. Kudler-Flam, S. Ryu, *Derivation of Holographic Negativity in AdS_3/CFT_2* , *Phys. Rev. Lett.* **123** (2019) 131603.
- [53] X. Dong, X.-L. Qi, and M. Walter, *Holographic entanglement negativity and replica symmetry breaking*, arXiv:2101.11029.
- [54] H. Shapourian, S. Liu, J. Kudler-Flam and A. Vishwanath, *Entanglement negativity spectrum of random mixed states: A diagrammatic approach*, arXiv:2011.01277.
- [55] S. Vardhan, J. Kudler-Flam, H. Shapourian and H. Liu, *Bound entanglement in thermalized states and black hole radiation*, [arXiv:2110.02959 [hep-th]].
- [56] J. Kudler-Flam, V. Narovlansky, and S. Ryu, *Negativity Spectra in Random Tensor Networks and Holography*, arXiv:2109.02649.
- [57] X. Dong, S. McBride and W. W. Weng, *Replica Wormholes and Holographic Entanglement Negativity*, [arXiv:2110.11947 [hep-th]].
- [58] P. Chaturvedi, V. Malvimat and G. Sengupta, *Holographic Quantum Entanglement Negativity*, *JHEP* **05**, (2018) 172.
- [59] P. Chaturvedi, V. Malvimat and G. Sengupta, *Covariant holographic entanglement negativity*, *Eur. Phys. J. C* **78** (2018) 776.
- [60] V. Malvimat and G. Sengupta, *Entanglement negativity at large central charge*, arXiv:1712.02288.
- [61] P. Jain, V. Malvimat, S. Mondal and G. Sengupta, *Holographic entanglement negativity conjecture for adjacent intervals in AdS_3/CFT_2* , *Phys. Lett. B* **793** (2019) 104.
- [62] P. Jain, V. Malvimat, S. Mondal and G. Sengupta, *Covariant holographic entanglement negativity for adjacent subsystems in AdS_3/CFT_2* , *Nucl. Phys. B* **945** (2019) 114683.
- [63] V. Malvimat, S. Mondal, B. Paul and G. Sengupta, *Holographic entanglement negativity for disjoint intervals in AdS_3/CFT_2* , *Eur. Phys. J. C* **79** (2019) 191.
- [64] V. Malvimat, S. Mondal, B. Paul and G. Sengupta, *Covariant holographic entanglement negativity for disjoint intervals in AdS_3/CFT_2* , *Eur. Phys. J. C* **79** (2019) 514.
- [65] V. Malvimat, S. Mondal and G. Sengupta, *Time Evolution of Entanglement Negativity from Black Hole Interiors*, *JHEP* **05** (2019) 183.
- [66] P. Chaturvedi, V. Malvimat and G. Sengupta, *Entanglement negativity, Holography and Black holes*, *Eur. Phys. J. C* **78** (2018) 499.
- [67] P. Jain, V. Malvimat, S. Mondal and G. Sengupta, *Holographic entanglement negativity for adjacent subsystems in $AdS_d + 1/CFT_d$* , *Eur. Phys. J. Plus* **133** (2018) 300.
- [68] J. Kumar Basak, H. Parihar, B. Paul and G. Sengupta, *Holographic entanglement negativity for disjoint subsystems in $AdS_d + 1/CFT_d$* , arXiv:2001.10534.
- [69] J. Kumar Basak, D. Basu, V. Malvimat, H. Parihar and G. Sengupta, *Page Curve for Entanglement Negativity through Geometric Evaporation*, arXiv:2106.12593.

- [70] J. Basak, D. Basu, V. Malvimat, H. Parihar and G. Sengupta, *Islands for Entanglement Negativity*, arxiv:2012.03983.
- [71] D. Basu, H. Parihar, V. Raj and G. Sengupta, *Defect extremal surfaces for entanglement negativity*, [arXiv:2205.07905 [hep-th]].
- [72] M. Afrasiar, J. Kumar Basak, A. Chandra and G. Sengupta, *Islands for Entanglement Negativity in Communicating Black Holes*, [arXiv:2205.07903 [hep-th]].
- [73] J. Lin and Y. Lu, *Effective reflected entropy and entanglement negativity for general 2D eternal black holes*, [arXiv:2204.08290 [hep-th]].